Detrital zircon U Pb age distributions and Hf isotopic constraints of the Ailaoshan-Song Ma Suture Zone and their paleogeographic implications for the Eastern Paleo-Tethys evolution

Qiuli Li, Wei Lin, Yin Wang, Michel Faure, Lingtong Meng, Hao Wang, Vuong van Nguyen, Hoai Luong Thi Thu, Claude Lepvrier, Yang Chu, et al.

Detrital zircon U-Pb age distributions and Hf isotopic constraints of the Ailaoshan-Song Ma Suture Zone and their paleogeographic implications for the Eastern Paleo-Tethys evolution

Qiuli Li, Wei Lin, Yin Wang, Michel Faure, Lingtong Meng, Hao Wang, Vuong Van Nguyen, Hoai Luong Thi Thu, Claude Lepvrier, Yang Chu, Wei Wei, Tich Van Vu

PII: S0012-8252(21)00290-7

DOI: https://doi.org/10.1016/j.earscirev.2021.103789

Reference: EARTH 103789

To appear in: *Earth-Science Reviews*

Received date: 30 March 2021

Revised date: 30 August 2021

Accepted date: 31 August 2021

Please cite this article as: Q. Li, W. Lin, Y. Wang, et al., Detrital zircon U-Pb age distributions and Hf isotopic constraints of the Ailaoshan-Song Ma Suture Zone and their paleogeographic implications for the Eastern Paleo-Tethys evolution, *Earth-Science Reviews* (2018), https://doi.org/10.1016/j.earscirev.2021.103789

Detrital zircon U-Pb age distributions and Hf isotopic constraints of the Ailaoshan-Song Ma Suture Zone and their paleogeographic implications for the Eastern Paleo-Tethys evolution

Qiuli Li[a,b], Wei Lin[a,b,*] linwei@mail.iggcas.ac.cn, Yin Wang[a,b,*], Michel Faure[c], Lingtong Meng[a,b], Hao Wang[a,b], Vuong Van Nguyen[d], Hoai Luong Thi Thu[d], Claude Lepvrier[e], Yang Chu[a,b], Wei Wei[a,b], Tich Van Vu[d]

[a]State Key Laboratory of Lithospheric Evolution, Institute of Geology and Geophysics, Innovation Academy of Earth Science, Chinese Academy of Sciences, Beijing 100029, China

[b]College of Earth and Planetary Sciences, University of Chinese Academy of Sciences, Beijing 100049, China

[c]Institut des Sciences de la Terre d'Orléans, UMR CNRS 7327, Université d'Orléans, 45067 Orléans Cedex 2, France

[d]Faculty of Geology, Hanoi University of Science, Hanoi, Vietnam

[e]Institut des Sciences de la Terre de Paris, UMR CNRS 7193, Case 129, Université Pierre & Marie Curie, 75252 Paris Cedex 05, France

[*]Corresponding author.

Abstract

During the Late Paleozoic to Cenozoic, with the closure of the Tethys oceans, the East and/or Southeast Asia was amalgamated by individual blocks. In order to understand the Paleogeography of the Eastern Paleo-Tethys, a systematic U-Pb dating on 11 samples have conducted to constrain the age and provenance of the elements forming the Ailaoshan-Song Ma mélange. These samples consist of the ophiolitic mélange zone (6 samples), the sedimentary cover of the Indochina block (4 samples), and the post-orogenic continental deposits (1 samples). The achieved detrital zircon age distribution, and the corresponding in-situ Hf isotopic recorder allow us to discuss the provenances of the materials involved in the tectonic processes during the subduction and collision. Three units (M1, M2, M3), which stand for the different segment of the suture zone, could be separated based on the differences in zircon age clusters and Hf isotopic values. These differences might be due to the variety of

provenances. Combined with the previous works, especially our work on the Song Chay mélange zone, we concluded that both upper and lower plates are potential provenances for the mélanges between South China block and Indochina block. Along the suture zone, the component of the mélange presents a significant heterogeneity.

Keyword Eastern Paleo-Tethys, Ailaoshan-Song Ma Suture, Detrital zircon, in-situ Hf isotopic content, Mélange, Tectonic evolution of SE Asia

1. Introduction

Sedimentary provenance analysis is a popular method and an effective tool to study the evolution of an orogenic belt as well as the erosion, the transport and finally the deposition processes in the foredeep basins (e.g. Fedo et al., 2003; Cawood et al., 2007, 2012; Dickinson and Gehrels, 2009). Ideally, the analyzed sample would completely represent geological history by including evidence of all the possible provenances. Detrital zircon geochronology has received particular attention as a single-mineral provenance tool because the abundance of zircon (in terms of numbers of grains) does not change drastically during sediment transport, owing to the inherent stability of zircon. The in situ Hf-isotope analysis of single zircon grains has proven to be a useful tool for reconstructing the tectonic evolution of continental blocks (Griffin et al., 2000; Condie et al., 2009). Therefore, the age spectra and related geochemistry, established from a large number of detrital zircon grains of igneous origin, could be used to constraints the ages of sedimentary sequences, to assess the provenance, and the routing of sediments through temporal/spatial dimensions. Such an approach requires a good knowledge of the magmatic, metamorphic, and tectonic events that took place in the source regions (Condie et al., 2009). Conversely, the analysis of detrital zircon age spectra might help to improve the understanding of the geological evolution of the source areas by revealing unexpected, or poorly documented magmatic or metamorphic events. This method has been widely applied in various orogenic belts, for instance the Tethyan & Alpine-Himalayan orogenic belts (Gehrels et al., 2011; Cai et al., 2016; Chu et al., 2016; Malusà et al., 2016; Lin et al., 2018; Metcalfe, 1996, 2002, 2011, 2013, 2021). The European Variscan-Appalachian belt is well investigated in Iberia (e.g. Martínez Catalán et al., 2008, 2009 and references

therein), the Bohemian massif (e.g. Henderson et al., 2016; Linnemann et al., 2004, 2007), Amorican (Lin et al., 2019), and Variscan Corsica (Avigad et al., 2018). As a syntectonic sedimentary formation, resulting of erosion, transportation and deposition in active settings, turbiditic matrix of the ophiolitic mélange records much information, such as uplift and tectonic phases that were erased by the late events of the corresponding orogenic belt (Henderson et al., 2018).

In Southwest China-North Vietnam region, several ophiolitic mélange zones, namely Ailaoshan-Song Ma, Song Chay and Song Hien/Dian-Qiong zones, have been proposed as the suture zones between South China Block (SCB) and Indochina Block (IB), representing the remnants of the Paleo-Tethys ocean (Figs. 1 and S1; Zhong, 1998; Trung et al., 2006; Sone & Metcalfe, 2008; Cai and Zhang, 2009; Lepvrier et al., 2011; Halpin et al., 2016). According to the Paleogeography, correlationpetrology of the mafic and ultramafic rocks, regional geochronology framework, different model related the closing of the Paleo-Tethys ocean were proposed: 1) Stampfli and Borel (2002) proposed Paleo-Tethys was a giant ocean whose width increased to the east. 2) An archipelagic ocean with numerous islands or seamount, which was situated between the Laurasia to the north and the Gondwana to the south (Liu et al.,1993, 2002; Pan et al., 1996); 3) the Paleo-Tethys served as a “conveyor belt”, in which several plates with different scale, such as Tarim, Qaidam, North Qiangtang, South Qiangtang, Lhasa, India, Sibumasu, Indochina, and South China etc…, were moved northwardly and finally accreted on the south margin of Laurasia accordingly (Becker and Faccenna, 2011); 4) An entirely continent-locked ocean in which a Cathaysian bridge uniting various elements of China and Indochina into an isthmian link between Laurasia and Gondwana-Land during the latest Permian, inhibiting any deep-sea connection between the Paleo-Tethys and the Panthalassa (Şengör and Atayman, 2009; Richards and Şengör, 2017). Based on structural geology and kinematic analyses, Faure et al. (2016) united the three ophiolitic mélange zones as a single suture zone duplicated by the Cenozoic Red River strike slip fault during the Cenozoic extrusion of Sundaland. However, the comparison of the detrital components between these three ophiolitic mélange zones is weak. A systematic U-Pb geochronological analysis and in-situ Hf isotopic on 11 samples have been realized to constrain the age and provenance of the elements forming the Ailaoshan-Song Ma mélange zone. The achieved detrital zircon age distribution, and the corresponding in-situ Hf isotopic recorder allow us to discuss the provenances of the materials involved in the tectonic processes during the subduction and collision. Our new data suggests a complicated source of

ophiolitic mélange, together with the published data in this region, this study shed new light on the understanding the paleogeographic reconstructions of the postulated positions of Asian continental blocks since Early Carboniferous to Middle Triassic.

2. Geological setting

As a significant Indosinian orogenic belt between SCB and IB, it was consisted by the Ailaoshan belt in NW and Song Ma belt in SE (Lepvrier et al., 2008; Faure et al., 2014, 2016). Each part could be subdivided into several individual tectonic zone.

2.1. The Ailaoshan belt

The Red River fault (RRF, Fig. 1) does not represent the plate boundary between Indochina and S. China blocks. This continental scale sinistral strike-slip fault, sometimes referred to as the "Ailaoshan-Red River shear zone" is a Cenozoic intracontinental feature that accommodated the southeastward extrusion of Sundaland with respect to Asia (e.g. Leloup et al., 1995; Wang et al., 2020). In contrast, plate boundaries decorated by ophiolites or ophiolitic mélanges are exposed in the Ailaoshan, Song Ma, and Song Chay areas in Yunnan, NW Vietnam, and NE Vietnam, respectively (Fig. 2).

Between the Ailaoshan and Song Ma segments, the structural continuity of the Indosinian orogen is partly hidden beneath the post-collisional red continental deposits and the N-S striking dextral Dien Bien Phu fault (Fig. 2). Several NW-SE striking Cenozoic sinistral strike-slip faults divide the belt into narrow stripes. The Ailaoshan belt is classically subdivided into four litho-tectonic zones, namely: Western Ailaoshan, Central Ailaoshan, Eastern Ailaoshan, and Jinping zones (Fig. 1, for details, see Zhong, 1998; Lai et al., 2014a, b; Faure et al., 2016).

2.1.1. The Western Ailaoshan zone: a magmatic arc

This zone is well exposed to the SW of Mojiang area (Fig. 2). From bottom to top, it is characterized by: i) an alternation of mudstone-sandstone turbiditic with Silurian-Devonian age, ii) a ca. 5 km-thick volcanic and volcanic-sedimentary series of Late Carboniferous-Late

Permian age (e.g. Fan et al., 2010; Lai et al., 2014a); Late Triassic red beds of conglomerate, sandstone, and siltstone that unconformably overlie the previous two series. The volcanic, greywacke and volcanic-clastic rocks are interpreted as formed in a volcanic arc setting since the geochemical signatures of the andesitic, dacitic, and basaltic lavas (Fan et al., 2010). The basalts and basaltic-andesites yield zircon SHRIMP ages at 287 ± 5 Ma, and 265 ± 7 Ma, respectively (Jian et al., 2009b; Fan et al., 2010). Dolerite and rhyolite yield zircon LA-ICP-MS ages at 246 ± 4 Ma, and 273 ± 5 Ma, 288 ± 3 Ma (Lai et al., 2014a). Moreover, close to the NW Vietnam belt, the granite to granodiorite plutons correspond to the root of the western Ailaoshan magmatic arc with zircon U-Pb ages at 257-252 Ma (Fig. 2; Lai et al., 2014a; Liu et al., 2015).

2.1.2. The Central Ailaoshan suture zone: an ophiolitic mélange

To the NW of the Mojiang city, a ca. 5 km wide domain with numerous m- to km-sized blocks or lenticular of serpentinized lherzolite and harzburgite, gabbro, plagiogranite, basalt, limestone, and Early Carboniferous radiolarite (with Albaillella paradoxa Deflandre, Astorentactinia multispinisa Won) enclosed into a metamorphosed sandstone-mudstone matrix crops out (Fig. 2; Zhong, 1998). Sandstone-mudstone alternations with turbiditic aspect can be frequently observed when the syn-metamorphic deformation is weak. This lithological assemblage is interpreted as pieces of dismembered ophiolitic mélange (e.g. Zhong, 1998; Yumul et al., 2008; Lai et al., 2014b; Faure et al., 2016).

Zircon from plagiogranite of the central Ailaoshan zone yields Late Devonian (365 ± 7 Ma, Lai et al., 2014b) and Early Carboniferous (328 ± 16 Ma, Jian et al., 1998a) ages. Diabase dykes are dated at 351 ± 11 Ma, and 334 ± 6 in this area (Lai et al., 2014b). These Devonian to Carboniferous magmatism was considered as coeval with the opening of the Paleo-Tethys (Jian et al., 1998b; Wu et al., 2020). Moreover, a late Early Triassic to early Middle Triassic felsic magmatism is documented in several places of the Central Ailaoshan zone. The leucogranite is dated at 247 ± 3 Ma (Liu et al., 2014), and the biotite granites yield ca. 244 Ma zircons (Lai et al., 2014a). Near Lüchun, the felsic magmatism is represented by rhyolites, tuffs, and pyroclastites. The rhyolite is dated at 246 ± 6 Ma (Fig. 2; Lai et al., 2014b). These 250-240 Ma magmatic rocks were interpreted as indicators of syn-collisional crustal melting.

2.1.3. The Eastern Ailaoshan zone: the deformed SCB

East of the Central Ailaoshan ophiolitic mélange, orthogneiss, paragneiss, amphibolite, and marble belong to a Neoproterozoic basement, corresponding to the SCB. Amphibolite yield zircon LA-ICP-MS ages at 815-800 Ma (Cai et al., 2015), whereas gneiss is dated around 770-750 Ma (Qi et al., 2012, 2014). Moreover, a younger age around 230 Ma is obtained from porphyritic granites (Lin et al., 2012).

2.1.4. The Jinping zone: a piece of the ELIP

Close to the NW Vietnam Song Ma belt, the Jinping zone is limited by Neogene strike-slip faults (Fig. 2). This zone is formed by Ordovician-Silurian limestone, and Silurian-Devonian turbidite. However, the most representative lithologies of the Jinping zone consist of Late Permian mafic rocks such as gabbro, basalt, basaltic breccia, pyroclastite and greywacke (Chung and Jahn, 1995; Xiao et al., 2004; Wang et al., 2007). The mafic magmatic rocks present mainly an alkaline geochemical signature (Wang et al., 2007). This lithological succession is similar to that recognized in the Song Da zone of NW Vietnam (c.f. below), and more widely to the Emeishan Large Igneous Province (Faure et al., 2016).

Involved in the Indosinian orogeny, the Jinping zone experienced the same deformation event as the Eastern Ailaoshan zone and belongs to the lower plate of the collision zone, despite that the lithology of the two discussed areas differ with each other.

2.2. The Song Ma belt

The Song Ma belt could be subdivided into the Truong Son-Sam Nua zone, Song Ma zone, Nam Co unit and fold and thrust zone tectonically (Fig. 2; Faure et al., 2014). Ophiolites or ophiolitic mélanges are exposed in the Song Ma zone (Fig. 2; Hutchison, 1975; Findlay and Trinh, 1997; Tran and Vu, 2011). The Song Ma belt was considered the “classical Suture zone” between Indochina and South China block (e.g. Wang et al., 2021 and therein). From the SW to the NE, several litho-tectonic zones are recognized.

2.2.1. Truong Son-Sam Nua zone: a magmatic arc

In the north of the Indochina Block, the wide occurrence of late Paleozoic to early Mesozoic igneous belt has been reported along the boundary of Laos and Vietnam (Fig. 1;

Lepvrier et al., 2008; Liu et al., 2012; Kamvong et al., 2014; Qian et al., 2019; Hou et al., 2019). At the north of Laos, the Sam Nua zone consists of Permian to Early Triassic volcanic and volcanic-clastic sedimentary series. Several plutons form a NW-SE striking magmatic belt that develops from east of the Dien Bien Fu fault, through the Sam Nua in Laos, up to the margin of the South China sea (Fig. 4). Tectonically, this magmatic belt located in the SW part of the Song Ma suture zone is interpreted as the magmatic arc formed during the southward subduction of the Paleo-Tethys (Fig.1; Tran et al., 2008; Rossignol et al., 2018). The geochronological data reveal that the felsic magmatism occurred from the Carboniferous to the Triassic (ca. 310-240 Ma) with a magmatic gap at ca. 270-265 Ma. Before the magmatic quiescent period, during the early magmatic stage (310-270 Ma), most of granitoids have low $^{87}Sr/^{86}Sr(i)$ and $\delta^{18}O$ values, high-$Mg^{\#}$, I-type with positive ε_{Nd} (t) and ε_{Hf} (t) values (Qian et al., 2019). These geochemical features are put forward to interpret the Truong Son granitoids as derived from the malting of a crustal source with a significant mantle contribution (Kamvong et al., 2014; Hoa et al., 2008). During the late magmatic stage, at 265-240 Ma, the magmatism consists of peraluminous I-type and abundant S-type granitoids of low-$Mg^{\#}$ and enriched Hf isotopes (Fig. 4). This suggests that the source of the magma was derived from the melting of an ancient continental crust without obvious mantle contribution (Liu et al., 2012; Qian et al., 2019).

2.2.2. The Song Ma suture zone: an ophiolitic mélange

This zone is formed by ultramafic, mafic, deep marine sedimentary rocks variously metamorphosed (Lepvrier et al., 2004). The ophiolite mainly consists of peridotite, basalt and gabbro, and experienced greenschist- to lower amphibolite-facies metamorphism (Zhang et al., 2014). The geochemistry of the mafic rocks (gabbro, plagiogranite, amphibolite) suggests a MORB affinity that is interpreted as a fore arc ophiolites signature (Tran and Vu, 2011; Trung et al., 2006). Late Carboniferous Sm-Nd whole rock ages comprised between 340 Ma and 310 Ma are obtained from amphibolites and gabbros, whereas zircon and titanite in these mafic rocks yield Late Permian to Late Triassic TIMS and LA-ICP-MS ages (between 270 Ma and 210 Ma) (Pham et al., 2008, Liu et al., 2012; Nguyen et al., 2013).

In the Thanh Hoa area, (Fig. 3), the Nui Nua Massif (also named Nui Nua Complex) is a ca. 15 km massif of serpentinized harzburgite, dunite, gabbro, diabase, that represents the southeasternmost ophiolitic element of the Song Ma suture. Serpentinized harzburgite and dunite bodies occurring as lenticular blocks surrounded by deformed and weakly or non-

metamorphosed sedimentary rocks. In the outcrop, the serpentinite breccia, light colored sandstone and siltstone with volcanic elements, such as basalts and volcano-clastic formations surround the mafic-ultramafic rocks are interpreted as an ophiolitic mélange (Thanh et al., 2016; Fig. 5). In the Nui Nua serpentinized peridotite and its country rocks, the NW-SE striking foliation exhibits a vertical or steeply dipping angles ranging from 60° to 85° either to the north or south. Undeformed and unmetamorphosed late Triassic continental coarse-grained feldspar-quartz sandstone overlain the ophiolitic mélange. However, the unconformity is not directly observed.

South of the Song Ma fault, among the Song Chu (i.e. Chu river), reddish sandstone and greywacke, sometimes with an oblique stratification, are ascribed to the Ordovician-Silurian Song Ca formation in the 1/200 000 scale geological map. However, our new detrital zircon analyses (samples TH 13, 14) reveal the presence of ca 270 Ma and/or 245 Ma (Permian, Triassic) ages that argue for a younger age (see details below). Because these sedimentary rocks are intruded by the Truong Son granitoids, they are considered as deposited in the active continental margin of the Northern part of IB.

2.2.3. The Nam Co zone: the highly deformed SCB

Northeast of the Song Ma suture zone, the Nam Co zone forms the tectonic substratum of the ophiolitic mélange. It consists of Neoproterozoic and Paleozoic sandstone, siltstone, and limestone that experienced a MP/MT barrowian metamorphism. East of Dien Bien Fu, HP/LT mafic eclogites yield zircon U-Pb LA-ICMS, and monazite U-Th-Pb chemical ages at 230.5 ± 8 Ma, and 243 ± 4 Ma, respectively (Nakano et al., 2008, 2010; Zhang et al., 2013). The Nam Co zone corresponds to the highly deformed and metamorphosed passive margin of the SCB that overthrust the fold and thrust zone of the NW Vietnam orogen.

2.2.4. The fold and thrust zone: the weakly deformed SCB

This domain that develops from the Nam Co zone to the RRF is the widest one of the NW Vietnam belts. It consists of deformed and weakly metamorphosed Paleozoic sedimentary rocks. Fold vergences and kinematic indicators show a top-to-the NE movement. A bimodal magmatic association with alkaline basalts, rhyolites, and volcanic-clastic rocks is ascribed to the Late Permian Song Da-Tu Lê rift. It is worth to note that, alike for the Jinping

zone in the Ailaoshan belt, these rocks are not ophiolites but belong to the Emeishan intraplate magmatic province offset in the Cenozoic by the Red River fault (Tran et al., 2008; Tran and Vu, 2011).

3. Analytical procedures

3.1 U-Pb isotope measurements

Typical outcrop photos and microphotographs of analyzed samples are shown in Figs. 5 and 6. Zircons from the samples were separated by conventional heavy liquid and magnetic techniques, and then picked by hand under a binocular microscope. About 250 zircon grains were randomly selected from over 500 grains (total zircon grains less than 200 were all selected), and mounted in epoxy resin, and polished to expose the inner part of the zircon grains. Transmitted and reflected light were used to avoid cracks and inclusions, and cathodoluminescence (CL) images, obtained by a CAMECA electron microscope, were used to identify the morphology and internal texture of the zircon grains.

Zircon U-Pb age analyses were conducted by using an Agilent 7500a ICP-MS housed at the Institute of Geology and Geophysics, Chinese Academy of Sciences in Beijing (IGGCAS). Laser ablation was operated at a constant energy 80 mJ and at 10 Hz, with a spot diameter of 44 μm. Gas flow rate of highly purified He as the carrier gas was 0.7 L/mn; auxiliary gas Ar was 1.13 L/mn. Total acquisition time of one spot was 45 s. The details of analytical procedures were the same as those described by Xie et al. (2008). The standard zircons (91500 and GJ-1) were used to determine the U-Th-Pb ratios and absolute abundances of the analyzed zircon. Data were processed with the GLITTER program (van Achterbergh et al., 2001). The $^{206}Pb/^{238}U$ ages are used for zircons with concordant ages less than 1000 Ma, and $^{207}Pb/^{206}Pb$ ages are used for zircons when $^{206}Pb/^{238}U$ ages are older than 1000 Ma. Data plot was conducted by using the Density Plotter program (Vermeesch, 2012). In this study, ages with more than ± 10% discordance were excluded.

3.2 Zircon Lu-Hf Isotopes

In situ Hf isotopic analysis was carried out on a Neptune multi-collector ICP-MS equipped with a Geolas-193 laser ablation system at the Institute of Geology and Geophysics, Chinese Academy of Sciences (IGGCAS). The analyzed spots of Lu-Hf isotopic analysis were performed on the same places on previously analyzed zircon grains for U-Pb isotopes, and detailed analytical procedures were described by Wu et al. (2006). Measuring settings mainly include beam diameter of 44 μm, repetition rate of 6 Hz, and laser beam energy density of 100 mJ/cm^2 and ablation time of 30s. The Lu-Hf model age is calculated assuming a two-stage evolution since extraction of the crustal protolith from depleted mantle, the model age allows us to compare the sedimentary sequence and potential bedrock sources (Andersen et al., 2016). The calculation formulas of the $\varepsilon_{Hf}(t)$ and Hf model ages are provided in the supporting information S2.

4. Sample analytical and results

4.1 Sampling and petrography

11 samples (Fig. 2 and 3, Table 1) were collected from both Ailaoshan belt and Song Ma belt in southwest China and north Vietnam, respectively. In each sampling site, 1 blocks of sample has been taken when the rock is with coarse grain, while 2 or 3 blocks, which are not far from each other when the rock is with fine grain. In the latter situation, all the blocks were crushed, mixed and enriched zircon grains together in order to acquire enough zircon grains. Our samples were mainly from the ophiolitic mélange unit (matrix of a serpentinite block) and the corresponding sedimentary cover of Indochina block (Table 1). Except for TH03, which is the pelite and siltstone and represent the matrix of a serpentinite block (Table 1), the samples come from sandstone, or from the sandy interlayers in the shales in the sedimentary cover of IB, and muddy matrix of mélange. Three samples were collected in the Ailaoshan belt, two of them (AS103, AS147) are from the already recognized ophiolitic mélange unit, and the last one (AS79) is from the Silurian sedimentary rock which represents the cover of IB.

AS103 is a sericite schist (meta-sandstone) as the matrix of a serpentinite block in the Ailaoshan ophiolitic mélange zone. In the outcrop, a well-developed foliation can be

observed, suggesting an intense shearing (Fig. 5B). In the thin section, the foliation is defined by oriented muscovite and elongated quartz (Fig. 6B). The major components are muscovite (~ 5%) and quartz (~ 50%). The grain size of this sample is around 0.05-0.50 mm with a concentration about 0.1-0.3 mm. AS147 is a schistose sandstone in the Ailaoshan ophiolitic mélange zone and represents the matrix of the serpentinite block. In the outcrop, the sandstone interbedded with pelite (Fig. 5C). Its grain size ranges from 0.05-0.40 mm, and mostly in 0.2-0.3 mm. In thin section, the foliation is defined by oriented quartz (Fig. 6C). The major components are quartz (~ 70%) and lithic fragments (~ 20%), with a minor muscovite (< 3%). Considering that, the two samples were from the ophiolitic mélange unit, therefore they were the non-Smith strata. The depositional environment of these samples is hard to determine. In the outcrop, which is less deformed, the Bouma sequences could be observed indicating continental slop in a semi deep sea and deep sea environment (Hao et al., 1999).

AS79 is a medium-fine grained sandstone from the Silurian turbidite in Ailaoshan area (Fig. 5A), which represents the sedimentary cover of the Indochina block. This sandstone is poorly sorted, and angular. The grain size is around 0.05-0.30 mm with a concentration about 0.1-0.2 mm (Fig. 6A). The major detrital components are quartz, sedimentary rock fragments, and muscovite. In the section, the angular quartz represents about 70% of the detrital component, and lithic fragments and muscovite together < 20% (Fig. 6A). The sequence of this sample was considered to belong to hemipelagic (YNBGMR-Mojiang, 1976; Hao et al., 1999).

Eight samples were collected from Song Ma belt. Except for TH01, which is a Late Triassic coarse-grained sandstone and represents the post-orogenic continental deposits, four of them (TH03, TH05, TH11, TH12) are from the ophiolitic mélange unit, and considered as the matrix of mélange. The rest three samples (TH09, TH13, TH14) are the coarse-grained sandstone from the Silurian and Middle Triassic turbidites, which are interpreted as the sedimentary cover in the north margin of IB.

TH01 is a Late Triassic grey-dark coarse-grained feldspar-quartz sandstone (Fig. 5D) in Thanh Hoa area. Because of the absence of ductile deformation and metamorphism, those Late Triassic coarse sandstone was interpreted as the continental deposits (Tri and Vu, 2011). The grain size is around 0.10-1.00 mm and commonly 0.40-0.70 mm. In thin section, the coarse quartz grains represent 75%-80% of the detrital component. Plagioclase and mica are

rarely observed (Fig. 6D). The sequence of this sample was considered to belong to littoral facies or lacustrine facies (Tran and Vu, 2011).

TH03 is a pelite and siltstone collected from surrounding rocks of a serpentinite block in Thanh Hoa area (Fig. 5E). In thin section, this sample is composed by extra-fine-grained minerals (mostly <0.05 mm), the round quartz grains constitute about 50% of the detrital component (Fig. 6E). TH05 is a schistosed medium to fine grained sandstone corresponding to the matrix of the ophiolitic mélange (Fig. 5F). This poorly sorted sandstone has grain-size around 0.02-0.30 mm with a concentration of 0.10-0.20 mm (Fig. 6F). The major components are angular or sub-angular quartz, plagioclase, and lithic fragments. In thin section, the coarse-grained quartz represents nearly 60% of the component. Lithic fragments are ~ 30%, and plagioclase and muscovite are <5% (Fig. 6F). TH11 is an intensively sheared tuff with very thin interbedded pelite in the ophiolitic mélange (Fig. 5G). In thin section, the well-developed foliation is defined by elongated quartz, mica and chlorite. The grain size ranges from 0.1 mm to 0.8 mm, with a concentration around 0.3-0.5 mm (Fig. 6H). The major components are quartz (~ 60%), muscovite (~ 20%) and chlorite (<5%). TH12 is a coarse-medium grained schistosed sandstone from the matrix of the ophiolitic mélange (Fig. 5I). These three samples were considered from the mélange unit, and belong to the non-Smith strata. The depositional environment and facies of these samples are unclear.

TH09 is a medium to fine grained sandstone from the Middle Triassic turbidite in Than Hoa area (Fig. 5H). In the outcrop, these rocks are intensively weathered. This sample is composed of poorly sorted and angular quartz with grain size around 0.05-0.15 mm (Fig. 6G). TH13 and TH14 is a purplish red, coarse-grained sandstone from the “Silurian” Song Ca Formation in Thanh Hoa area (Fig. 3). The cross beddings observed in the outcrop suggest a normal sequence of this formation (Fig. 5J). Abundant muscovite and volcanic debris can be observed in the outcrop. TH09, TH13 and TH14 were considered from the forearc basin, the cross bedding and the well sorted grains suggest shallow-marine facies (Tran and Vu, 2011).

4.2 Zircon U-Pb results

Representative CL images of the analyzed zircons are shown in Fig. 7. Most of the zircon grains exhibit a sub-rounded to rounded shape indicating a relatively long transportation, and only a small part of grains are prismatic crystals. Most of the grains show a zonal structure, and some of the grains possess an inner core surrounded by recrystallization

rims. All the LA-ICP-MS U-Pb results of the eleven samples are provided in Tables S1 in the supporting information.

AS79: the detrital zircon grains mostly have a round shape with a length from 80 to 150 μm (Fig. 7A). A total of 74 analyses were undertaken in the 74 grains, and 63 results were concordant. The analyzed zircon grains also show oscillatory zoning in the CL image (Fig. 7A), indicating a magmatic origin. The concordant ages range from 425 to 3549 Ma, with two major peaks at 440 Ma and 970 Ma (Fig. 8A).

AS103: the detrital zircon grains are mostly round-shaped, transparent and colorless, with the length of 30 to 150 μm, most of which show oscillatory zoning in the CL image (Fig. 7B). Among the 90 analyses conducted on 90 zircon grains in this sample, 71 dated zircons have concordant ages. The concordant ages range from 371 to 3089 Ma with two major peaks at 430 Ma and 975 Ma and two subordinate peaks at 1050 Ma and 2480 Ma (Fig. 8B).

AS147: the detrital zircon grains of sample AS147 are round or prismatic shape, ranging from 50 to 200 μm (Fig. 7C). In this sample, a total of 91 spots on 91 grains were analyzed, and 79 concordant ages were obtained. Th/U ratios of these zircons range from 0.02 to 2.26, in which the majority have Th/U ratios higher than 0.1 (Table S1). Combined with the oscillatory zoning shown in the CL images (Fig. 7C), the Th/U ratios indicate a magmatic origin for them. These zircons yield the concordant ages ranging from 374 to 3231 Ma, which have peaks at 425 Ma, 965 Ma, 1730 Ma and 2520 Ma (Fig. 8C).

TH01: the analyzed grains range from 120 to 200 μm in length, with round or prismatic shape, and have length-width ratios of 1:1 to 3:1 (Fig. 7D). In this sample, a total of 100 spots from 97 grains was analyzed, and 95 analyzed results were concordant. These zircons have Th/U ratios ranging from 0.01 to 2.12 (Table S1). Apart from three grains, Th/U ratios of most grains are higher than 0.1, indicating a magmatic origin for the dated zircons. These zircons yield the concordant ages ranging from 217 to 2363 Ma. The concordant ages mainly cluster at 200 to 500 Ma with two significant peaks at 240 Ma and 440 Ma and show two subordinate peaks at 920 Ma and 2360 Ma (Fig. 8D).

TH03: a total of 163 spots on 163 grains were analyzed, and 53 analyses were concordant. Apart from one spot, other zircon have Th/U ratios higher than 0.1, ranging from 0.13 to 2.65. The measured concordant ages range from 223 to 2486 Ma (Table S1). One

major age group occurs at 220-400 Ma, showing two peaks at 240 Ma and 370 Ma (Fig. 8E). Two subordinate groups are also present at 700-1000 Ma with a peak at 780 Ma, and 1600-1800 Ma with a peak at 1750 Ma (Fig. 8E).

TH05: the detrital zircon grains are 50 to 200 μm in length with round or prismatic shape and have length-width ratios of 1:1 to 3:1 (Fig. 7F). 101 analytical spots were carried out on 101 zircon gains and yield 88 concordant ages ranging from 263 to 3426 Ma. All of these zircons have Th/U ratios higher than 0.1 with the range of 0.11 to 4.79 (Table S1). Two major age groups occur at 415-500 Ma and 800-1000 Ma with peaks at 440 Ma and 950 Ma (Fig. 8F). Two subordinate age peaks of 1865 Ma and 2425 Ma are also shown in the sample TH05 (Fig. 8F).

TH09: in this sample, detrital zircons are mostly round, transparent and colorless, ranging from 80 to 200 μm in length, with a length-width ratio of 1:1 to 2:1 (Fig. 7G). A total of 100 grains were analyzed, and 75 out of 100 spots have the concordant ages. Except one spot with Th/U ratio lower than 0.1, others have higher Th/U ratios with a range of 0.14 to 2.14 (Table S1). Combined with the oscillatory zoning revealed in the CL images, the Th/U ratios higher than 0.1 are indicative of a magmatic origin. The concordant ages range from 232 to 2721 Ma with two dominate peaks at 260 Ma and 450 Ma and one subordinate peak around 890 Ma (Fig. 8G).

TH11: the detrital zircon grains in this sample are 30 to 120 μm in length with round or prismatic shape and have length-width ratios of 1:1 to 2:1 (Fig. 7H). We analyzed 100 spots on 100 grains in this sample, and all of the results are concordant. Combined with the CL images, the Th/U ratios of dated zircons with a range of 0.07 to 1.59, mostly higher than 0.1, indicate a magmatic origin for these zircons (Fig. 7H and Table S1). Except the youngest age (TH11#60, 117 Ma), the concordant ages mainly cluster between 204 and 283 Ma with a significant peak at 247 Ma (Fig. 8H).

TH12: the detrital zircon grains of this sample are mostly round-shaped, transparent and colorless, which are 60 to 150 μm in length with length-width ratios of 1:1 to 2.5:1 and show oscillatory zoning in the CL image (Fig. 7I). 81 analyses were carried out on 78 zircon grains and 75 spots give concordant ages (Table S1). Apart from one spot with Th/U ratio of 0.07, others have Th/U ratios higher than 0.1, indicating a predominantly magmatic origin for these zircons. The concordant ages range from 224 to 1078 Ma, mostly clustering between 220 and

270 Ma. Hence, sample TH12 show a significant peak at 246 Ma and a subordinate peak at 740 Ma (Fig. 8I).

TH13: the detrital zircon grains are mostly round-shaped, transparent and colorless, with the length of 100 to 180 μm, most of which show oscillatory zoning in the CL image (Fig. 7J). In this sample, a total of 100 spots on 100 grains were analyzed, and 98 concordant ages were obtained. All of these zircons show Th/U ratios higher than 0.1 and range from 0.14 to 1.75 (Table S1). These Th/U ratios and morphometric features revealed by CL image are indicative of a magmatic origin for these zircons (Fig. 7J). The concordant ages range from 225 to 2517 Ma. The analyzed results fall into the range of 220-300 Ma and 350-450 Ma with a significant peak around 270 Ma and a subordinate peak at 440 Ma (Fig. 8J). A low background of dispersed ages from Early Paleozoic to Neoarchean is also demonstrated (Fig. 8J).

TH14: the detrital zircon grains selected from this sample for dating are mostly round or prismatic-shaped, transparent and colorless. They are about 30 to 80 μm in length with length-width ratios of 1:1 to 1.5:1 and show oscillatory zoning in the CL image (Fig. 7K). A total 100 analyses were carried out in 100 grains, and 73 results are concordant, ranging from 223 to 1879 Ma (Table S1). Th/U ratios of these zircons range from 0.01 to 1.56, in which more than 90% ones are higher than 0.1(Table S1). Two dominant age groups are documented at 250-280 Ma with a peak at 245 Ma and at 320-480 Ma with a peak at 385 Ma (Fig. 8K). One subordinate peak of 935 Ma is shown in the sample TH14 (Fig. 8K).

4.3 Zircon Lu-Hf isotopic analysis

Lu-Hf isotopic analysis were carried out on dated zircon grains, with analytical spots adjacent to those for U-Pb dating. The results of the U-Pb ages, ε_{Hf} (t) values and T_{DM}^{2} ages are plotted in Figs. 8, S1, 9 and 10. All the Lu-Hf results of eleven samples are provided in Table S2 in the supporting information.

AS79: in this sample, twenty-three grains from the dated zircons were chosen for in situ Hf isotope analyses. The ages of these detrital zircons are between 406 and 2042 Ma with $(^{176}Hf/^{177}Hf)_i$ ratios varying from 0.281516 to 0.282789 (Table S2). Accordingly, these zircon grains have $\varepsilon_{Hf}(t)$ values of -21.1 to +10.1 with peaks at -9.70 and 7.75 (Fig. S2A). The

calculated T_{DM}^2 ages of these zircons range from 764 to 3012 Ma, peaking at 870 Ma, 1970 Ma, 2530, and 2940 Ma (Fig. 9A).

AS103: in this sample, twenty-nine dated zircons were chosen for in situ Hf isotope analyses and yield $(^{176}Hf/^{177}Hf)_i$ ratios ranging from 0.281498 to 0.282706 (Table S2). Combined with their concordant ages of 421 to 2514 Ma, these zircons yield ε_{Hf} (t) values ranging from -23.3 to +24.2 with one major peak at -3.55 and two subordinate peaks at -21.2 and 5.55 (Fig. S2B). The T_{DM}^2 ages vary from 931 to 3268 Ma with clusters around 1470 Ma, 2030 Ma, 2350 Ma and 3020 Ma (Fig. 9B).

AS147: in this sample, thirty-six dated zircons were chosen for in situ Hf isotope analyses, which have the concordant ages of 413 to 2533 Ma. They show the $(^{176}Hf/^{177}Hf)_i$ ratios varying from 0.281171 to 0.282448 (Table S2). All the analyses have ε_{Hf} (t) values of -21.5 to +2.92 with peaks at -3.55, -10.2 and -20.6 (Fig. S2C). The zircon T_{DM}^2 ages have the range of 1541 to 3025 Ma, clustering around 1620 Ma, 2080 Ma, 2610 Ma and 2950 Ma (Fig. 9C).

TH01: in this sample, twenty dated zircons were chosen for in situ Hf isotope analyses, yielding the $(^{176}Hf/^{177}Hf)_i$ ratios varying from 0.281784 to 0.282650 (Table S2). Considering that the concordant ages of these zircons range between 239 and 976 Ma, we calculated εHf(t) values to be -14.1 to +3.95 with one major peak at -8.31 (Fig. S2D). The zircon T_{DM}^2 ages range of 1209 to 2682 Ma with a significant peak at 1950 Ma (Fig. 9D).

TH03: in this sample, twenty dated zircons with concordant ages of 237-2692 Ma were chosen for in situ Hf isotope analyses. They yield $^{176}Hf/^{177}Hf$ ratios varying from 0.281063 to 0.282719 (Table S2). Accordingly, the ε_{Hf} (t) values range from -26.2 to +7.5 with three peaks at -25.7, -10.9, and 1.35 (Fig. S2E). The zircon T_{DM}^2 ages vary from 925 to 3143 Ma, clustering at 1100 Ma, 1580 Ma, 2090 Ma, 2360 Ma, and 2940 Ma (Fig. 9E).

TH05: in this sample, twenty dated zircons were chosen for in situ Hf isotope analyses with the U-Pb ages of 431 to 2525 Ma. Their $(^{176}Hf/^{177}Hf)_i$ ratios vary from 0.280783 to 0.282792, and ε_{Hf} (t) values range from -15.7 to +10.3 with peaks at -9.35 and -3.05 (Table S2 and Fig. S2F). Accordingly, the zircon T_{DM}^2 ages were calculated to be 754 to 3915 Ma with one major peak around 1980 Ma and several subordinate peaks at 750 Ma, 1510 Ma, 2480 Ma, 3310 Ma and 3920 Ma (Fig. 9F).

TH09: in this sample, thirty-one dated zircons were chosen for in situ Hf isotope analyses, yielding the $(^{176}Hf/^{177}Hf)_i$ ratios with the range of 0.281535 to 0.282553 (Table S2). These zircons have concordant ages between 239 and 1760 Ma, mostly clustering between 240 and 500 Ma. Accordingly, their ε_{Hf} (t) values range from -30.3 to +29.1 with one major peak at -9.80 (Fig. S2G). The calculated T_{DM}^2 ages of these zircons range from 552 to 3283 Ma with one major peak at 2000 Ma and four subordinate peaks at 550 Ma, 1645 Ma, 2510 Ma, and 3270 Ma (Fig. 9G).

TH11: in this sample, ten dated zircons that have concordant ages around 247 Ma were chosen for in situ Hf isotope analyses. The $(^{176}Hf/^{177}Hf)_i$ ratios range from 0.282342 to 0.282773 (Table S2). All the analyses reveal the ε_{Hf} (t) values ranging from -10.3 to +5.15 with two dominant peaks at -8.45 and 3.15 (Fig. S2H). The calculated T_{DM}^2 ages of these zircons range from 925 to 1898 Ma, showing two peaks at 1020 Ma and 1800 Ma (Fig. 9H).

TH12: in this sample, in situ Hf isotope analyses carried out on twenty-two dated zircons show $(^{176}Hf/^{177}Hf)_i$ ratios ranging from 0.281771 to 0.282791 (Table S2). Combined their concordant ages of 234 to 1078 Ma, these zircons yield ε_{Hf} (t) values ranging from -11.7 to +5.95 with one major peak at -7.65 and 3.79 (Fig. S2I). The T_{DM}^2 ages vary from 879 to 2630 Ma with clusters around 1050 Ma, 1510 Ma, 1770 Ma and 2640 Ma (Fig. 9I).

TH13: in this sample, in situ Hf isotope analyses are carried on twenty zircons that have the concordant ages clustering at 250-450 Ma and three zircons with Proterozoic ages, yielding the $(^{176}Hf/^{177}Hf)_i$ ratios of 0.281591 to 0.282596 (Table S2). The ε_{Hf} (t) values vary from -27.5 to +14.2 with one significant peak at -2.15 (Fig. S2J). These zircons have T_{DM}^2 ages ranging from 1310 to 2996 Ma that have a major peak at 1430 Ma (Fig. 9J).

TH14: in this sample, due to the small size of these zircons, only thirteen results of situ Hf isotope analyses have been acquired. The $(^{176}Hf/^{177}Hf)_i$ ratios range from 0.281603 to 0.282616 (Table S2). Combined with their concordant ages of 242 to 1620 Ma, ε_{Hf} (t) values were calculated to be -23.6 to 3.12 with peaks at -11.4 and -6.12 (Fig. S2K). The calculated T_{DM}^2 ages range from 1178 to 2921 Ma, clustering around 1170 Ma, 1740 Ma, 2110 Ma, and 2800 Ma (Fig. 9K).

5. Discussion

5.1 Classification of the Ailaoshan-Song Ma mélange from the view of the detrital zircon

Based on our own data and previous detrital zircon works in the Ailaoshan-Song Ma ophiolitic mélange zone (Xia et al., 2016, 2020; Xu et al., 2019), we reinterpreted these results according to our understanding of the Indosinian orogeny. Three groups of samples reveal three mélange related units, M1, M2, and M3, respectively (Table 3). Namely, M1 unit: **AS103, AS147, TH05,** YN41, YN54 (the specimens in bold are belong to this study, the rest refer to Xia et al., 2016, 2020; and Xu et al., 2019) are characterized by two major age groups with peaks at around 435 Ma and 970 Ma (Fig. 11); M2 unit: AE02, AW06, AW07, AW08, AW10, is characterized by a major late Permian (260 Ma) age group with several unobvious Neoproterozoic-Paleozoic and Paleoproterozoic clusters (Fig. 11); and M3 unit: AW17, AW1720, 13YZ06, **TH03, TH11, and TH12**, is characterized by only one conspicuous Mesozoic age peak located at 250 Ma (Fig. 11).

The M1 unit mainly crops out in the middle segment of the Ailaoshan ophiolitic mélange (Fig. 2). In the 1:200,000 scale geological map, this unit was identified as Silurian sedimentary rocks (Fig. 2; YNBGMR-Mojiang, 1976). Our analytical results exhibit age peaks ranging from Neoarchean to early Paleozoic at 2510 Ma, 1860 Ma, 1690 Ma, 1085 Ma, 970 Ma, 810 Ma and 435 Ma (Fig. 11). Among them 970 Ma and 435 Ma are the two most significant peaks. A youngest cluster around 370 Ma (Famennian) indicates that the previously proposed stratigraphy deserves re-evaluation (Table 2; Fig. 11). The existence of the Late Paleozoic cluster suggests that the deposition of these rocks was younger than the previous stratigraphic attribution indicated in the geological map (YNBGMR-Mojiang, 1976). It is worth to mention, that the T_{DM}^2 of these analytical zircons indicates several peaks of Archean to Proterozoic with 1.55, 2.05, 2.35 and 2.95 Ga and the Phanerozoic zircon show the ε_{Hf} range from -15 ~ +10 (Figs. 12 and 13).

At the NW segment of the Ailaoshan ophiolitic mélange zone, the rocks ascribed here to the M2 unit are reclassified as parts of the mélange unit instead of the Permian strata in the 1:200,000 scale geological map (Fig. 2; YNBGMR-Mojiang, 1976; Jian et al., 1998a; Faure et al., 2014, 2016; Liu et al., 2015; Xia et al., 2016, 2020). Detrital zircons from this unit exhibit

a major age group at 250-280 Ma with peak at 260 Ma, and serval age minor groups with peaks at around 410 Ma, 770 Ma, 950 Ma, 1840 Ma, 2480 Ma (Xia et al., 2020). The two-stage model Hf age of these 280-240 Ma zircons indicate a significant peak of Neoproterozoic (0.85 Ga; Fig. 11). At the same time, the ε_{Hf} of the zircon with the ages between 260-240 Ma show ranges from -1 ~ +7 and indicates the parts of the material have mantle contribution (Figs. 12 and 13).

At the SE segment of the Ailaoshan and the Song Ma ophiolitic mélange zone, the M3 located at the NE of Song Ma fault. Our analytical results exhibit age ranging from Neoarchean to early Mesozoic with clusters around 1045 Ma, 770 Ma, 360 Ma, and 250 Ma (Fig. 11). Among them 250 Ma represents a conspicuous peak. A youngest cluster around 240 Ma (Ladinian, Table 2; Fig. 11) is also detected. This means that the deposition age of M3 is younger than Ladinian. The $\varepsilon_{Hf}(t)$ of the zircon with ages comprised between 250-235 Ma show ranges from -17 ~ -5 with the two-stage model ages mainly concentrated at 1.3 Ga to 1.8 Ga (Fig. 12), and indicates the material derived from ancient continental crust without significant mantle contribution (Fig. 13). These characters make the M3 different from the M1 and M2.

5.2 Source of Detrital Zircons of the Cover of North Indochina Block

In our samples, the AS79, TH02, TH13, and TH14 represent the Paleozoic sedimentary cover in the north Indochina block (Figs. 2, 3). These rocks are supposed to locate at the retro-belt (Doglioni et al., 2007; Doglioni and Panza, 2015). However, in the field, this tectonic event could not be fixed because of the intensive Cenozoic sinister strike-slip deformation.

The AS79 is a Middle Silurian sandstone from the West Ailaoshan belt, representing the sedimentary cover of the IB (YNBGMR-Mojiang, 1976). According to the result of detrital zircon U-Pb ages, the deposition age of sample AS79 was not older than 440 Ma (Table 2) and correspond well to the Middle Silurian strata age. The age spectrum of AS79 shows two major age groups of 400-500 Ma and 900-1000 Ma, which is almost the same with the results of the Silurian sedimentary rocks in Truong Son belt (Wang et al., 2016a). According to Wang et al. (2016a), the 400-500 Ma detrital zircons with age peak around 440 Ma originated from the magmatic rocks in Kontum massif. The 900-1000 Ma detrital zircons, showing subrounded to rounded shaped, were considered to derive from the magmatic rocks in the

Rayner-Eastern Ghats belt in India and Antarctic (Usuki et al., 2013; Wang et al., 2016a; Xia et al., 2016).

TH09 is a Middle Triassic medium to fine grained sandstone , the maximum deposition age of this sample is about 257 Ma, which is constrained by the youngest graphical age peak, youngest 1σ grain cluster, and youngest 2σ grain cluster (Table 2). Two major age groups of 230-290 Ma and 420-470 Ma were revealed in the age spectrum (Fig. 8G). The 230-290 Ma age group with peak at around 260 Ma detrital zircons yield negative ε_{Hf} value (Fig. 10), which corresponds to the magmatic rocks in the Truong Son belt (Figs. 4 and 16). Therefore, we consider that the 230-290 Ma detrital zircons recorded the detrital materials from the magmatic arc. The 420-470 Ma age group with peak at around 440 Ma may come from the magmatic rocks in Kontum massif or recycled from the Paleozoic sedimentary rocks in the north Indochina. Considering the euhedral zircons of this age group, we prefer to consider the magmatic rocks in Kontum massif as the main source.

TH13 is a coarse grain sandstone marked as "Silurian" in the local geological map (Fig. 3). However, according to the result of detrital zircon, the youngest graphical age peak, youngest 1σ grain cluster, and youngest 2σ grain cluster are much younger, around 270 Ma (Table 2). This result suggests that TH13 deposited later than 270 Ma, and a Late Permian age is assumed for this sample. The age spectrum exhibits a dominated cluster at around 270 Ma and a minor group around 440 Ma, together with the euhedral morphology of the zircons, suggests a nearby provenance of these zircons. Like TH09, the 270 Ma group is considered to derived from the magmatic rocks of the Truong Son belt, and the 440 Ma age group could come from the magmatic rocks in the Kontum massif.

TH14 is a "Silurian" coarse sandstone close to TH13. The age spectrum shows two main age peaks and a minor one at around 245 Ma and 385 Ma, and 935 Ma, respectively. The deposition age of this sample is younger than 242 Ma (Anisian), which suggests a late Middle Triassic age of this sample. The 200-300 Ma age group detrital zircons probably come from the magmatic rocks of the Truong Son belt. As for the 350-450 Ma detrital zircons with age peaks at ~ 385 Ma, although there is no contemporaneous magmatic record in Indochina, the Ailaoshan ocean opened in this period (Zhong, 1998; Jian et al., 2009a), and the missing rift related magmatism can be the potential provenance of the age group detrital zircons.

5.3 Sources of detrital zircons of the Ailaoshan-Song Ma Suture Zone

5.3.1 Provenance of detrital zircons in M1 unit

The age pattern of the detrital zircon in M1 is characterized by two dominant age groups at 400-450 Ma and 930-1000 Ma, with age peaks at around 435 Ma and 970 Ma respectively (Figs. 11 and 14). This age distribution is highly consistent with the results of detrital zircon ages yielded from the Silurian sedimentary rocks, which were considered as the cover of IB (Zhong, 1998; Tri and Vu, 2011; Xia et al., 2016), in Eastern Simao or Truong Son belt (IB, Figs. 1 and15). Furthermore, similar detrital zircon age patterns are also reported in the Late Paleozoic sedimentary rocks in both in IB and Cathaysia Block (Wang et al., 2014; Xia et al., 2016; Wang et al., 2016a; Fig. 15). These Paleozoic sedimentary rocks are potential sources for the M1 unit. The $\varepsilon_{Hf}(t)$ values of the 400-450 Ma age group in M1 range from -19.6 to +10.3, yet most (84.2%) of data are negative, and the corresponding model ages range from 0.75 Ga to 2.61Ga (Fig. 10). The distributions of $\varepsilon_{Hf}(t)$ values and model age are in agreement with the results from the Silurian sedimentary rocks in Eastern Simao (Fig. 1; Xia et al., 2016), therefore we tend to regard the Silurian sedimentary rocks in Eastern Simao as the main source of the M1 unit. Even so, we cannot exclude the 400-450 Ma magmatic rocks in northern Kontum massif as the potential sources of this group of detrital zircons (Wang et al., 2021 and references therein). As for the youngest cluster zircons around 370 Ma in the M1 unit (Table 2), contemporary gabbro, plagiogranite and diabase, considered to relate with the opening of Paleo-Tethys, had been widely reported in the Ailaoshan-Song Ma ophiolitic mélange zone (Jian et al., 2009a; Zhong et al., 2013; Lai et al., 2014a; Zhang et al., 2014). Based on this hypothesis, there would be contemporary acid magmatism although it has not been reported before, therefore these Late Devonian acid magmatic rocks can be also a potential provenance of the youngest Late Paleozoic cluster zircons. It is worth to note that all the M1+M2+M3 mélanges contain these Late Devonian zircons.

5.3.2 Provenance of detrital zircon in M2 unit

The age pattern of the detrital zircon in M2 unit is relatively simple and dominated by a 240-270 Ma age group. In addition, five minor age groups with peaks at around 410 Ma, 770 Ma, 950 Ma, 1840 Ma, and 2480 Ma have been recognized in the M2 (Fig. 11; Xia et al., 2020). It is worth to note that the minor age spectrum in the M2 was consistent with the age pattern of M1 (Fig. 11). Therefore, we interpret the component with these minor age groups in

M2 as mainly recycled from the sedimentary rocks in IB. This hypothesis is supported by the high similarity of the detrital zircon age distributions between the M2 and the Late Permian Longtan Formation in Eastern Simao, IB (Fig. 15; Xia et al., 2020).

As for the dominant 240-270 Ma age group in M2, the corresponding $\varepsilon_{Hf}(t)$ values and model ages of detrital zircon range from -28.9 to +8.1 and 2.53 Ga to 0.67 Ga respectively. According to Xia et al. (2020), the dominant 240-270 Ma age group represents the detrital material from the magmatic arc. However, there is another possibility that this group of detrital zircons originated from the Emeishan Large Igneous Province (ELIP, characterized by basaltic magmatism with subordinate rhyolites, granites and syenites, Xu et al., 2008), which was as a major magmatic event that occurred mainly between 250-270 Ma in the western margin of the SCB (Xu et al., 2008). Considering the Cenozoic large scale strike slip of the Ailaoshan shear zone (Tapponnier, et al., 1990; Leloup et al., 1995), it is reasonable to consider that the ELIP supplied the detrital material to the M2. This hypothesis could be identified by: 1) the highly similarity of $\varepsilon_{Hf}(t)$ values and model ages from the 240-270 Ma detrital zircons in M2 and the zircons in ELIP (Figs. 12 and13); 2) the $\varepsilon_{Hf}(t)$ values and model ages of the 240-270 Ma detrital zircons from the Late Permian Longtan Formation, which was considered to record the detrital material directly from the magmatic arc (Xia et al., 2020), are highly similar with those from ELIP (Fig. 16); 3) most importantly, the $\varepsilon_{Hf}(t)$ values and model ages of the magmatic zircons from Western Ailaoshan-Truong Son belt are significantly different with the detrital zircons from both M2 unit and Late Permian Longtan Formation (Fig. 17). These lines of hints suggest that the 240-270 Ma detrital zircons, at least half of them (positive $\varepsilon_{Hf}(t)$ values, 52%), may come from the ELIP, rather than the magmatic arc as previously suggested (Xia et al., 2020).

5.3.3 Provenance of detrital zircons in M3 unit

Similar with M2 unit, the age spectrum of the detrital zircon in M3 unit shows a dominant age group and two minor age groups. However, the dominant age group with an age peak around 245 Ma in M3 is slightly younger than that in M2 unit (Table 2), besides, the two minor age groups yield age peaks at around 370 Ma, and 780 Ma. The dominant 230-260 Ma age group yields $\varepsilon_{Hf}(t)$ values and two-stage model Hf age between -21.9 to 10.1 and 0.55 Ga to 2.62 Ga respectively (Figs. 12 and 13). In this cluster, most of 84.8% of the $\varepsilon_{Hf}(t)$ values

are negative, which is significantly different from that in M2 (Fig. 13). On the contrary, the $\varepsilon_{Hf}(t)$ values and model ages in M3 unit are highly consistent with those yielded by the 230-260 Ma magmatic arc in western Ailaoshan-Truong Son belt (Fig. 16). Therefore, this dominant cluster in M3 unit recorded the detrital material directly supplied by the western Ailaoshan-Truong Son magmatic arc. This hypothesis is also supported by the widespread magmatism during 245-255 Ma in the western Ailaoshan-Truong Son magmatic arc belt (Fig. 16).

As discussed above, the cluster with age peak around 370 Ma may record the detrital material from the magmatic rocks coeval with the opening of Paleo-Tethys, similar with the case in M3 unit. However, the age group with peak at ~ 780 Ma was documented from the Paleozoic sedimentary rock in both the IB (including Simao) and southwest margin of SCB (Xia et al., 2016; Wang et al., 2016a; Zhou et al., 2018). Besides, the contemporary igneous rocks are widely reported in the southwest margin of the SCB (Li et al., 2002; Li, 2003a, 2003b; Huang et al., 2008; Wang et al., 2011; Cai et al., 2015; Chen et al., 2017; Li et al., 2018) Nevertheless, we tend to consider that this detrital zircon age group originated from the southwest margin of the SCB, rather than IB, for the following reasons: 1) the 780 Ma cluster appears as a major age group of the Paleozoic sedimentary rocks in southwest margin of the SCB, and just a minor one in IB; 2) the characteristic age peaks at around 440 Ma and 960 Ma of the IB are missing in the M3 unit, which suggests that the Paleozoic sequences in IB may not supply the material of the M3 unit; 3) the rounded to subrounded shapes of this age group zircons (Fig. 7) indicate a long transportation or a polycyclic history of the grains, this means that the 780 Ma age group zircons probably not directly originated from the igneous rocks in the southwest margin of SCB. Moreover, the M3 unit deposited in the Middle Triassic when the Paleo-Tethys ocean was almost closed, thus it is quite possible that the detrital material of the SCB deposited in the subduction zone.

5.4 Source of Detrital Zircons of the Late Triassic continental deposits

In our samples, the TH01 is the Late Triassic coarse sandstone, unconformably resting upon the Nui Nua Complex, Thanh Hoa ophiolitic mélange, was interpreted as the post-collisional continental deposits (Tran and Vu, 2011). The age pattern shows two main age groups of 220-270 Ma and 410-470 Ma (Fig. 8D). A minor age groups with age peaks around 920 Ma is also detected (Fig. 8D). This age pattern is similar to the results from the Late Triassic sedimentary in Sam Nua basin (Rossignol et al., 2018), therefore a similar

provenance for the TH01 can be inferred. According to Rossignol et al. (2018), the provenance of the 200-300 Ma detrital zircons was attributed to the post-collisional magmatic rocks in Truong Son belt and the 400-500 Ma detrital zircons derived from the magmatic rocks in Kontum massif or recycled from the Paleozoic sedimentary rocks.

5.5 Comparison of the Ailaoshan-Song Ma and Song Chay ophiolitic mélange

The Song Chay ophiolitic mélange is a discontinuous zone, exposed as discrete patches along the Song Chay fault, NE of the Day Nui Con Voi. This mélange zone was recognized and proposed as a suture zone from long-time (Şengör et al. 1988; Lepvrier et al., 2011). Wang et al. (2021) have analyzed the detrital zircons from the matrix of Song Chay ophiolitic mélange. This study revealed that the detrital zircon yields several age peaks from Paleoproterozoic to Late Paleozoic, at 2440 Ma, 1775 Ma, 1560 Ma, 970Ma, 770 Ma, 730 Ma, 620 Ma, 460 Ma, and 310 Ma (Fig. 14). The widely represented Indosinian (240-260 Ma) detrital zircons in the M2 and M3 units are missing in the Song Chay mélange, and on the contrary, the dominant 700-800 Ma cluster in the Song Chay mélange is very limited in the three units of the Ailaoshan-Song Ma ophiolitic mélange (Figs. 8, 11, and 13). This significant difference between the Ailaoshan-Song Ma and Song Chay ophiolitic mélange suggests different provenances for these two ophiolitic mélanges (Fig. 14). The provenance of the detrital zircon in the Song Chay mélange was interpreted as mainly from the SCB, with only a very limited amount of Late Paleozoic zircons that might come from the IB (Wang et al.,2021). Therefore, we speculate that the differences in the age patterns of detrital zircon in the Song Chay and Ailaoshan-Song Ma ophiolitic mélanges reflect the variety of the sources that supplied the material deposited in the subduction mélange all along the segments of the Ailaoshan-Song Ma-Song Chay suture. This interpretation agrees with what is also identified in the Ailaoshan-Song Ma ophiolitic mélange zone by the different M1, M2, and M3 units (Fig. 14).

5.6 Tectonic implications

It is well known that at least from Middle Devonian, several blocks were separated from the Northern Gondwana, drifted to the north, and accreted onto the Laurasia, along with the

opening and closure of the Paleo-Tethys (Figs. 17A and 18A). Combined our detrital zircon work and previous geochronological, geochemical and structural geology works in this region, during the Late Carboniferous to Early Permian (310-270 Ma), the Paleo-Tethys begin to close. This process was accommodated by a south-directed subduction and made a NW-SE striking Western Ailaoshan-Truong Son magmatic arc belt along the north margin of IB (e.g. Hoa et al., 2008; Liu et al., 2012; Shi et al., 2015; Wang et al. 2018). The geochemical features (low $^{87}Sr/^{86}Sr_{(i)}$ and $\delta^{18}O$ values, high-Mg$^{\#}$, I-type with positive ε_{Nd} (t) and ε_{Hf} (t)) indicated the early stage of the magmatism and were often interpreted as typical for the subduction process (the A1 in Fig. 16; Hoa et al., 2008; Fan et al., 2010; Li, 2012; Kamvong et al., 2014; Lai et al., 2014a, 2014b; Hieu et al., 2016; Wang et al., 2016b, 2018; Hou et al., 2019; Qian et al., 2019; Jiang et al., 2020). During this time, along the Song Chay segment, the magmatic arc was less developed, and the SCB (as the passive margin) acted as the main provenance of sediments in the mélange (Figs. 14, 17B; Wang et al., 2021). On the contrary, in the western part of Western Ailaoshan-Truong Son magmatic arc belt (IB), the Upper Permian (Longtan formation), as the sediments of retro-arc basin, contain significant signal of these period (yellow cross in Fig. 16). For the future zone of Ailaoshan-Song Ma belt, it seems that the magmatic arc did not provide material as the source of the ophiolitic mélange (Fig. 11). As mentioned above (5.3.1), we argue that the sedimentary cover of the Eastern Simao as the main source of the M1 unit (Fig. 17B'). During the 270-265 Ma interval, Western Ailaoshan-Truong Son magmatic arc belt experienced a magmatically quiet period (Fig. 4). Generally, this quiescent period was interpreted as the tectonic transition from subduction to initial collision, which reasonably accounts for the change in the petrogenetic types and magma sources of the associated igneous rocks (Qian et al., 2016, 2019; Hou et al., 2019). After the magmatic gap, the magmatic arc began to develop again in Western Ailaoshan-Truong Son belt, which could supply numerous zircons to the mélange. However, the ELIP also developed during this time and the acid magmatism could also provide a large number of zircons and act as the source of the mélange. Even we cannot exclude the provenance of M2 unit from the Longtan formation of Eastern Simao (Xia et al., 2020), the highly similarity of ε_{Hf}(t) values and model ages from the 240-270 Ma detrital zircons in M2 and the zircons in ELIP make us to conclude that the provenance of M2 may come from the ELIP of the SCB (A2 in Fig. 16; Fig. 17C). On the period of the 260-240 Ma, from the view of the ε_{Hf}(t) values and model ages in M3, the provenance of the component of the mélange was supplied from the magmatic arc in western Ailaoshan-Truong Son magmatic arc belt (Fig. 16). As discussed in the section 5.3.3, a part of the component in M3 came from the

passive margin of the SCB, and this support the provenance of M3 from the both sides of the suture zone (Fig. 17D).

The different components and provenances of the Song Chay ophiolitic mélange, Song Ma ophiolitic mélange and Ailaoshan ophiolitic mélange suggest a lateral heterogeneity of the Ailaoshan-Song Ma-Song Chay suture. The SCB acted as the main provenance for the Song Chay ophiolitic mélange, which indicates that the Paleo-Tethys ocean in the Song Chay segment was a narrow ocean (Wang et al., 2021). However, the sedimentary cover in IB and the magmatic arc was the main source of the Ailaoshan and Song Ma ophiolitic mélanges, except the M2 unit, limited detrital zircons were considered to derive from SCB, this may suggest a relatively wide ocean basin separating the SCB and IB. Therefore, we consider that this branch of the Paleo-Tethys ocean was narrowing eastward.

Based on this hypothesis, a paleogeographic reconstructions of the postulated positions of Asian continental blocks from Early Carboniferous to Middle Triassic is proposed in Fig. 18. The opening of the Ailaoshan-Song Ma-Song Chay ocean was considered to take place in the Middle Devonian (Zhong, 1998; Jian et al., 2009a), and the Indochina block began to travel northward due to the opening of another southern branch of the Paleo-Tethys (Figs. 17A and 18A). During the ocean spreading period (380-310 Ma), the Ailaoshan-Song Ma-Song Chay ocean became a wedge-shape ocean narrowing eastward (Fig. 18A). The Ailaoshan-Song Ma-Song Chay ocean began to subduct southward during Late Carboniferous and lead to the 310-270 Ma magmatic arc documented in the Western Ailaoshan-Truong Son belt (Figs. 4, 16, 17B and 18C). During this time, the Paleo-Tethys ocean in the Song Chay area was a narrow ocean, the detrital material from the SCB was supplied in the Song Chay ophiolitic mélange (Figs. 17B and 18B). However, in the Ailaoshan-Song Ma area, the detrital material from the SCB was not transported to the trench possibly because of the wideness of the ocean basin (Figs. 17B' and 18B). The 270-260 Ma magmatic quiescence in the Western Ailaoshan-Truong Son magmatic arc belt was interpreted as due to the initial collision between the SCB and IB (Qian et al., 2016, 2019; Hou et al., 2019). The eruption of the ELIP in this period provided abundant zircons, which supplied the clastic material in the M2 unit of the Ailaoshan-Song Ma ophiolitic mélange zone (Figs. 17C and 18C). During the Upper Permian to Lower Triassic (260-240 Ma), the SCB continued to subduct (Fig. 17D), and the second stage magmatic rocks began to develop (Figs. 4, 16 and 17D). At this time, the SCB and IB were amalgamated together (Figs. 17D and 18D). The Late Triassic magmatic

rocks in Western Ailaoshan-Truong Son magmatic arc belt (Figs. 4 and 16) were interpreted as the post-collisional magmatism (Liu et al., 2012; Lai et al., 2014b; Hieu et al., 2016).

6. Conclusion

Detrital zircon U-Pb dating results from eleven samples in the Ailaoshan-Song Ma suture zone demonstrate major age peaks at 245 Ma, 440 Ma, and 970 Ma that correspond to the tectonic events recognized in SCB and IB. In-situ Hf isotopic results indicate that these Neoproterozoic and Early Paleozoic events represent significant continental growth episodes with mantle addition. Along the suture zone, the ophiolitic mélange zone have been subdivided into M1, M2, and M3 units based on the differences in zircon age and Hf isotopic signature. M1 is characterized by two major age groups with peaks at around 435 Ma and 970 Ma, the source of M1 is likely the Paleozoic sedimentary cover (especially Silurian sedimentary rocks) in IB mainly, with a very small amount from magmatic rocks in the ophiolitic mélange. M2 is characterized by a dominant late Permian (260 Ma) age group with the $\varepsilon_{Hf}(t)$ values ranging from -1 ~ +7 and a significant peak at ~ 0.85 Ga of model ages, the source of M2 is considered dominantly from the ELIP and related rocks in SCB with a very small number of detrital zircons derived from recycled sedimentary rocks in IB. M3 is characterized by only one conspicuous Mesozoic age peak located at 250 Ma with the $\varepsilon_{Hf}(t)$ values ranging from -17 ~ -5 and the two-stage model ages mainly concentrated at 1.3 Ga to 1.8 Ga, the M3 material was dominantly supplied from the magmatic arc in IB (Western Ailaoshan-Truong Son belt) with a very small amount from southwest margin of the SCB. The distinction of these three units shown above indicates a significant lateral heterogeneity along the suture zone. Our data shed new light on the understanding the paleogeographic reconstructions of the postulated positions of Asian continental blocks from the Early Carboniferous to the Middle Triassic.

Acknowledgements

We thank the Editor in Chief Carlo Doglioni and two reviewer Walter Mooney and Udo Zimmermann are deeply for their constructive comments and suggestions, which lead to a great improvement of our manuscript. This work has been financially supported by the

National Natural Science Foundation of China (91855212 and 91755205) and the National Key R&D Program of China (2016YFC0600102 and 2016YFC0600401).

Declaration of interest statement

No conflict of interest exits in the submission of this manuscript. All the authors listed have approved the manuscript that is enclosed. Neither the entire paper nor any part of its content has been published or has been accepted elsewhere. It is not being submitted to any other journal at the same time.

References

Avigad, D., Rossi, Ph., Gerdes, A., Abbo, A., 2018. Cadomian metasediments and Ordovician sandstone from Corsica: detrital zircon U-Pb-Hf constrains on their provenance and paleogeography. Int. J. Earth Sci. 107, 2803-2818.

Backer, T.W., Faccenna, C., 2011. Mantle conveyor beneath the Tethyan collisional belt. Earth Planet. Sci. Lett. 310, 453-461.

Backhouse, D., 2004. Geological Setting, Alteration and Nature of Mineralization at the Phu Kham Copper-Gold Deposit, Laos PDR. Unpublished. B.Sc. thesis. University of Tasmania, Hobart, pp. 141.

Cai, F.L., Ding, L., Laskowski, A.K., Kapp, P., Wang, H., Xu, Q., Zhang, L., 2016. Late Triassic paleogeographic reconstruction along the Neo-Tethyan Ocean margins, southern Tibet. Earth Planet. Sci. Lett. 435, 105-114.

Cai, J.X., Zhang, K.J., 2009. A new model for the Indochina and South China collision during the Late Permian to the Middle Triassic, Tectonophysics 467(1-4), 35-43.

Cai, Y., Wang, Y., Cawood, P.A., Zhang, Y., Zhang, A., 2015. Neoproterozoic crustal growth of the Southern Yangtze Block: Geochemical and zircon U-Pb geochronological and Lu-Hf isotopic evidence of Neoproterozoic diorite from the Ailaoshan zone. Precambrian Res. 266, 137-149.

Cawood, P.A., Hawkesworth, C.J., Dhuime, B., 2012. Detrital zircon record and tectonic setting. Geology 40(10), 875-878, doi: 10.1130/G32945.1

Cawood, P.A., Nemchin, A.A., Strachan, R.A., Prave, A.R., and Krabbendam, M., 2007. Sedimentary basin and detrital zircon record along East Laurentia and Baltica during

assembly and breakup of Rodinia: J. Geol. Society 164, 257-275, doi:10.1144/0016-76492006-115

Chen, Q., Sun, M., Long, X., Zhao, G., Wang, J., Yu, Y., Yuan, C., 2018. Provenance study for the Paleozoic sedimentary rocks from the west Yangtze block: constraint on possible link of south china to the Gondwana supercontinent reconstruction. Precambrian Res. 309, 271-289.

Chen, Q., Sun, M., Long, X., Zhao, G., Yuan, C., 2016. U-Pb ages and hf isotopic record of zircons from the late Neoproterozoic and Silurian-Devonian sedimentary rocks of the western Yangtze block: implications for its tectonic evolution and continental affinity. Gondwana Res. 31, 184-199.

Chen, X., Liu, J., Fan, W., Qi, Y., Wang, W., Chen, J., Burg, J.-P., 2017. Neoproterozoic granitoids along the Ailao Shan-Red River belt: Zircon U-Pb geochronology, Hf isotope analysis and tectonic implications. Precambrian Res. 299, 244-263.

Chu, Y., Lin, W., Faure, M., Wang, Q., 2016. Detrital zircon U-Pb ages and Hf isotopic constraints on the terrigenous sediments of the Western Alps and their paleogeographic implications. Tectonics 35, doi:10.1002/2016TC004276

Chung, S.L., Jahn, B.M., 1995. Plume-lithosphere interaction in generation of the Emeishan flood basalts at the Permian-Triassic boundary. Geology 23(10): 889-892.

Condie, K.C., Belousova, E., Griffin, W.L., Sircombe, K.N., 2009. Granitoid events in space and time: constraints from igneous and detrital zircon age spectra. Gond. Res. 15, 228-242.

Cromie, P.W., 2010. Geological setting, geochemistry and genesis of the Sepon gold and copper deposits, Laos. Unpublished Ph. D thesis. University of Tasmania, Hobart, pp.395. 228-242.

Dickinson, W.R., Gehrels, G.E., 2009. Use of U-Pb ages of detrital zircons to infer maximum depositional ages of strata: A test against a Colorado Plateau Mesozoic database. Earth Planet. Sci. Lett. 288(1-2), 115-125. doi:10.1016/j.epsl.2009.09.013

Doglioni C., Carminati E., Cuffaro M. and Scrocca D., 2007. Subduction kinematics and dynamic constraints. Earth Sci. Rev. 83, 125-175, doi:10.1016/j.earscirev.2007.04.001.

Doglioni C. and Panza G.F. (2015) Polarized plate tectonics. Advances in Geophysics 56, 3, 1-167.

Dong, Y., Sun, S., Santosh, M., Zhao, J., Sun, J., He, D., Shi, X., Hui, B., Cheng, C., Zhang, G., 2021. Central China Orogenic Belt and amalgamation of East Asian continents. Gondwana Res. doi:10.1016/j.gr.2021.03.006

Duan, L., Meng, Q.-R., Christie-Blick, N., Wu G.-L., 2017. New insights on the Triassic tectonic development of South China from the detrital zircon provenance of Nanpanjiang turbidites. Geol. Soc. Am. Bull. 130(1-2), 24-34.

Fan, W.M., Wang, Y.J., Zhang, A.M., Zhang, F.F., Zhang, Y.Z., 2010. Permian arc-back-arc basin development along the Ailaoshan tectonic zone: geochemical, isotopic and geochronological evidence fromthe Mojiang volcanic rocks, Southwest China. Lithos 119, 553-568.

Faure, M., Lepvrier, C., Nguyen, V.V., Vu, V.T., Lin, W., Chen, Z., 2014. The South China block-Indochina collision: where, when, and how? J. Asian Earth Sci. 79, 260-274.

Faure, M., Lin, W., Yang, C., Lepvrier, C., 2016. Triassic tectonics of the southern margin of the South China Block. Compt. Rendus Geosci. 328, 5-14.

Fedo, C.M., Sircombe, K.N., Rainbird, R.H., 2003. Detrital zircon analysis of the sedimentary record. In: Hanchar, J.M., Hoskin, P.W.O. (Eds.) Zircon. Rev. in Min. and Geochem. 53, 277-303.

Findlay, R.H., Pham, T.T., 1997. The structural setting of the Song Ma region, Vietnam and the Indochina-South China plate boundary problem. Gondwana Res. 1, 11-33.

Gehrels, G., Kapp, P., DeCelles, P., Pullen, A., Blakey, R., Weislogel, A., Ding, L., Guynn, J., Martin, A., McQuarrie, N., Yin, A., 2011. Detrital zircon geochronology of pretertiary strata in the Tibetan-Himalayan orogen. Tectonics 30, TC5016. doi:10.1029/2011TC002868

Griffin, W.L., Pearson, N.J., Belousova, E.A., Jackson, S.E., van Achterbergh, E., O'Reilly, S.Y., Shee, S.R., 2000. The Hf isotope composition of cratonic mantle: LAM-MC-ICPMS analyses of zircon megacrysts in kimberlites. Geochim. et Cosmochimi. Acta 64, 133-147.

Halpin, J.A., Tran, H.T., Lai, C.-K., Meffre, S., Crawford, A.J., Zaw, K., 2016. U-Pb zircon geochronology and geochemistry from NE Vietnam: A 'tectonically disputed' territory between the Indochina and South China blocks. Gondwana Res. 34, 254-273.

Hao, Z.W, Rao, R.B., Xu, X.Q. Yao, D.S., Fang, F.L., 1999. Regional stratigraphy in Southwest China. Wuhan, Publishing House China University of Geosciences, p. 220. (in Chinese with English abstract)

Henderson, B.J., Collins, W.J., Murphy, J.B., Alonso, G., Handa, M., 2016. Gondwanan basement terranes of the Variscan-Appalachian orogen: Baltican, Sahara and West African hafnium isotopic fingerprints in Avalonian, Iberia and Armorican Terranes. Tectonophysics 681, 278-304.

Henderson, B.J., Collins, W.J., Murphy, J.B., Hand, M., 2018. A hafnium isotopic record of magmatic arcs and continental growth in the Iapetus Ocean: the contrasting evolution of Ganderia and the peri-Laurentian margin. Gond. Res. 58, 141-160.

Hieu, P.T., Chen, F., Nguyen, T.B.T., Nguyen, Q.C., Li, S.Q., 2013. Geochemistry and zircon U-Pb ages and Hf isotopic composition of Permian alkali granitoids of the Phan Si Pan zone in northwestern Vietnam. J. Geodyn. 69, 106-121.

Hieu, P.T., Li, S.-Q., Yu, Y., Thanh, N.X., Dung, L.T., Tu, V.L., Siebel, W., Chen, F., 2016. Stages of late Paleozoic to early Mesozoic magmatism in the Song Ma belt, NW Vietnam: evidence from zircon U-Pb geochronology and Hf isotope composition. Int. J. Earth Sci. 106(3), 855-874.

Hoa, T.T., Anh, T.T., Phuong, N.T., Dung, P.T., Anh, T.V., Izokh, A.E., Borisenko, A.S., Lan, C.Y., Chung, S.L., Lo, C.H., 2008. Permo-Triassic intermediate-felsic magmatism of the Truong Son belt, eastern margin of Indochina. Compt. Rendus Geosci. 340, 112-126.

Hou, L., Liu, S., Guo, L., Xiong, F., Li, C., Shi, M., Zhang, Q., Xu, S., Wu, S., 2019. Geology, geochronology, and Hf isotopic composition of the Pha Lek Fe deposit, northern Laos: implications for early Permian subduction-related skarn Fe mineralization in the Truong Son belt. J. Earth Sci. 30, 109-120.

Hu, L., Cawood, P.A., Du, Y., Xu, Y., Wang, C., Wang, Z., Ma, Q., Xu, X., 2017. Permo-Triassic detrital records of South China and implications for the Indosinian events in East Asia. Palaeogeogr. Palaeoclimatol. Palaeoecol. 485, 84-100.

Hu, L., Cawood, P.A., Du, Y., Xu, Y., Xu, W., Huang, H., 2015. Detrital records for Upper Permian-Lower Triassic succession in the Shiwandashan Basin, South China and implication for Permo-Triassic (Indosinian) orogeny. J. Asian Earth Sci. 98, 152-166.

Hu, L., Du, Y., Cawood, P.A., Xu, Y., Yu, W., Zhu, Y., Yang, J., 2014. Drivers for late Paleozoic to early Mesozoic orogenesis in South China: constraints from the sedimentary record. Tectonophysics 618, 107-120.

Huang, X.-L., Xu, Y.-G., Li, X.-H., Li, W.-X., Lan, J.-B., Zhang, H.-H., Liu, Y.S., Wang, Y.B., Li, H.Y., Lou, Z.Y., Yang, Q.J., 2008. Petrogenesis and tectonic implications of Neoproterozoic, highly fractionated A-type granites from Mianning, South China. Precambrian Res. 165, 190-204.

Hutchison, C.S., 1975. Ophiolites in Southeast Asia. Geol. Soc. Am. Bull. 86, 797-806.

Jian, P., Liu, D., Kroner, A., Zhang, Q., Wang, Y., Sun, X., Zhang, W., 2009a. Devonian to Permian plate tectonic cycle of the Paleo-Tethys Orogen in southwest China (I):

geochemistry of ophiolites, arc/back-arc assemblages and within-plate igneous rocks. Lithos 113, 748-766.

Jian, P., Liu, D., Kroner, A., Zhang, Q., Wang, Y., Sun, X., Zhang, W., 2009b. Devonian to Permian plate tectonic cycle of the Paleo-Tethys Orogen in southwest China (II): insights from zircon ages of ophiolites, arc/back-arc assemblages and within-plate igneous rocks and generation of the Emeishan CFB province. Lithos 113, 767-784.

Jian, P., Wang, X., He, L., Wang, C., 1998a. U-Pb zircon dating of the Shuanggou ophiolite from Xingping County, Yunnan Province. Acta Petrol. Sin. 14, 207-212 (in Chinese with English abstract).

Jian, P., Wang, X.F., He, L.Q., Wang, C.S., 1998b. Geochronology of ophiolite rocks from the Ailaoshan suture, Yunnan province, southwestern Yunnan province, southwestern China: implications of Palaeotethyan evolution (in Chinese with English abstract). Geol. Miner. Resour. South China 1, 1-11.

Kamvong, T., Zaw, Khin, Meffre, S., Maas, R., Stein, H., Lai, C., 2014. Adakites in the Truong Son and Loei fold belts, Thailand and Laos: genesis and implications for geodynamics and metallogeny. Gondwana Res. 26, 165-184.

Lai, C.-K., Meffre, S., Crawford, A.J., Zaw, K., Halpin, J.A., Xue, C.-D., Salam, A., 2014a. The Central Ailaoshan ophiolite and modern analogs. Gondwana Res. 26, 75-88.

Lai, C.-K., Meffre, S., Crawford, A.J., Zaw, K., Xue, C.-D., Halpin, J.A., 2014b. The Western Ailaoshan Volcanic Belts and their SE Asia connection: a new tectonic model for the Eastern Indochina Block. Gondwana Res. 26, 52-74.

Leloup, P.H., Lacassin, R., Tapponnier, P., Schärer, U., Zhong, D.L., Liu, X.H., Zhang, L.S., Ji, S.C., Phan, T.T., 1995. The Ailao Shan-Red River shear zone (Yunnan, China), Tertiary transform boundary of Indochina. Tectonophysics 251, 3-84.

Lepvrier, C., Faure, M., Van Vuong, N., Van Vu, T., Lin, W., Thang, T.T., Phuong, T.H., 2011. North-directed Triassic nappes in Northeastern Vietnam (East Bac Bo). J. Asian Earth Sci. 41, 56-68.

Lepvrier, C., Maluski, H., Van Tich, V., Leyreloup, A., Truong Thi, P., Vuong, N.V., 2004. The Early Triassic Indosinian orogeny in Vietnam (Truong Son Belt and Kontum Massif); implications for the geodynamic evolution of Indochina. Tectonophysics 393, 87-118.

Lepvrier, C., Maluski, H., Van Vuong, N., Roques, D., Axente, V., Rangin, C., 1997. Indosinian NW-trending shear zones within the Truong Son belt (Vietnam): 40Ar-39Ar Triassic ages and Cretaceous to Cenozoic overprints. Tectonophysics 283, 105-127.

Lepvrier, C., Van Vuong, N., Maluski, H., Thi, P.T., Van Vu, T., 2008. Indosinian tectonics in Vietnam. Compt. Rendus Geosci. 340, 94-111.

Li, X., Li, Z., Ge, W., Zhou, H., Li, W., Liu, Y., Wingate, M.T.D., 2003a. Neoproterozoic granitoids in South China: crustal melting above a mantle plume at ca. 825 Ma? Precambrian Res. 122, 45-83.

Li, X.-C., Zhao, J.-H., Zhou, M.-F., Gao, J.-F., Sun, W.-H., Tran, M., 2018. Neoproterozoic granitoids from the Phan Si Pan belt, Northwest Vietnam: Implication for the tectonic linkage between Northwest Vietnam and the Yangtze Block. Precambrian Res. 309, 212-230.

Li, X.-H., Li, Z.-X., Zhou, H., Liu, Y., Kinny, P.D., 2002. U-Pb zircon geochronology, geochemistry and Nd isotopic study of Neoproterozoic bimodal volcanic rocks in the Kangdian Rift of South China: implications for the initial rifting of Rodinia. Precambrian Res. 113, 135-154.

Li, Y., 2012. Granites geochemical characteristics and Era research of the Skarn-type iron ore deposit In Laos Pa. Master thesis, China University of Geosciences (Beijing), Beijing, pp. 49. (in Chinese with English abstract)

Li, Z., Li, X., Kinny, P.D., Wang, J., Zhang, S., Zhou, H., 2003b. Geochronology of Neoproterozoic syn-rift magmatism in the Yangtze Craton, South China and correlations with other continents: evidence for a mantle superplume that broke up Rodinia. Precambrian Res. 122, 85-109.

Lin, T.H., Chung, S.L., Chiu, H.Y., Wu, F.Y., Yeh, M.W., Searle, M., Iizuka, Y., 2012. Zircon U- Pb and Hf isotope constraints from the Ailao Shan-Red River shear zone on the tectonic and crustal evolution of southwestern China. Chem. Geol. 291, 23-37.

Lin, W., Faure, M., Li, X. H., Ji, W., 2019. Pre-Variscan tectonic setting of the south margin of Armorica: Insights from detrital zircon ages distribution and Hf isotopic composition of the St-Georges-sur-Loire Unit (S. Armorican Massif, France). Tectonophysics 766, 340-378.

Lin, W., Rossi, P., Faure, M., Li, X., Ji, W., Chu, Y., 2018. Detrital zircon age patterns from turbidites of the Balagne and Piedmont nappes of Alpine Corsica (France): evidence for an European margin source. Tectonophysics 722, 69-105.

Linnemann, U., Gerdes, A., Drost, K., Buschmann, B., 2007. The continuum between Cadomian orogenesis and opening of the Rheic Ocean: Constraints from LA-ICP-MS U-Pb zircon dating and analysis of plate-tectonic setting (Saxo-Thuringian zone, NE Bohemian massif, Germany). In: Linnemann, U., Nance, R.D., Kraft, P., Zulauf, G.

(Eds.), The Evolution of the Rheic Ocean: From Avalonian-Cadomian Active Margin to Alleghenian-Variscan Collision: Geol. Soc. Am. Spec. Paper, vol. 423. pp. 61-96.

Linnemann, U., McNaughton, N.J., Romer, R.L., Gehmlich, M., Drost, K., Tonk, C., 2004. West African provenance for Saxo-Thuringian (Bohemian Massif): did Armorica ever leave pre-Pangean Gondwana? U/Pb-SHRIMP zircon evidence and the Nd-isotopic record. Int. J. Earth Sci. 93, 683-705.

Liu B.P., Feng, Q.L., Chonglakman, C., Helmcke, D., 2002. Framework of Paleotethyan archipelago ocean of western Yunnan and its elongation towards north and south. Earth Sci. Front. 9(3), 161-171. (in Chinese with English abstract)

Liu, B.P., Feng, Q.L., Fang, N.Q., Jia, J.H., He, F.X., 1993. Tectonic evolution of Paleao-Tethys poly-island-ocean in Changning-Menglian and Lancangjiang belts, southwestern Yunnan, China. J. Earth Sci. 18(5), 529-539. (in Chinese with English abstract)

Liu, H., Wang, Y., Cawood, P.A., Fan, W., Cai, Y., Xing, X., 2015. Record of Tethyan ocean closure and Indosinian collision along the Ailaoshan suture zone (SW China). Gondwana Res. 27, 1292-1306.

Liu, H.C., Wang, Y., Fan, W.M., Zi, J.W., Y.I. Y.G.L., C., 2014. Petrogenesis and tectonic implications of Late-Triassic high εNd(t)-εHf(t) granites in the Ailaoshan tectonic zone (SW China). Sci. China 57, 2181-2194.

Liu, J.L., Tran, M., Tang, Y., Nguyen, Q.L., Tran, T.H., Wu, W., Chen, J., Zhang, Z., Zhao, Z., 2012. Permo-Triassic granitoids in the northern part of the Truong Son belt, NW Vietnam: geochronology, geochemistry and tectonic implications. Gondwana Res. 122, 628-644.

Malusà, M.G., Anfinson, O.A., Dafov, L.N., Stockli, D.F., 2016. Tracking Adria indentation beneath the Alps by detrital zircon U-Pb geochronology: Implications for the Oligocene-Miocene dynamics of the Adriatic microplate. Geology 44, 155-158.

Manaka, T., 2014. A study of mineralogical, geochemical and geochronological characteristics and ore genesis in Phuoc Son Gold deposit area, Central Vietnam. Published Ph. D thesis. University of Tasmania, Hobart, pp. 207.

Martinez Catalan, J.R., Arenas, R., Abati, J., Sanchez Martinez, S., Diaz Garcia, F., Fernandez Suarez, J., Gonzalez Cuadra, P., Castineiras, P., Gomez Barreiro, J., Diez Montes, A., Gonzalez Clavijo, E., Rubio Pascual, F.J., Andonaegui, P., Jeffries, T.E., Alcock, J.E., Diez Fernandez, R., Lopez Carmona, A., 2009. A rootless suture and the loss of the roots of a mountain chain: the Variscan belt of NW Iberia. Compt. Rendus Geosci. 341, 114-126.

Martinez Catalan, J.R., Fernandez-Suarez, J., Meireles, C., Gonzalez-Clavijo, E., Belousova, E., Saeed, A., 2008. U-Pb detrital zircon ages in synorogenic deposits of the NW Iberian Massif (Variscan belt): interplay of Devonian-Carboniferous sedimentation and thrust tectonics. Int. J. Earth Sci. 165, 687-698.

Metcalfe, I., 1996. Pre-Cretaceous evolution of SE Asian terranes. In: Hall, R., Blundell, D. (Eds.), Tectonic Evolution of Southeast Asia. Geol. Soc. Spec. Publ. 106, 97-122.

Metcalfe, I., 2002. Permian tectonic framework and palaeogeography of SE Asia. J. Asian Earth Sci. 20(6), 551-566.

Metcalfe, I., 2011. Palaeozoic-Mesozoic history of SE Asia. Geol. Soc. Spec. Publ. 355(1), 7-35.

Metcalfe, I., 2013. Gondwana dispersion and Asian accretion: tectonic and palaeogeographic evolution of eastern Tethys. J. Asian Earth Sci. 66, 1-33.

Metcalfe, I., 2021. Multiple Tethyan ocean basins and orogenic belts in Asia. J. Asian Earth Sci. doi:10.1016/j.gr.2021.01.012

Nakano, N., Osanai, Y., Minh, N.T., Miyamoto, T., Hayasaka, Y., Owada, M., 2008. Discovery of high-pressure granulite-facies metamorphism in northern Vietnam: Constraints on the Permo-Triassic Indochinese continental collision tectonics. Compt. Rendus Geosci. 340(2-3), 127-138.

Nakano, N., Osanai, Y., Sajeev, K., Hayasaka, Y., Miyamoto, T., Minh, N.T., Owada, M., 2010. Triassic eclogite from northern Vietnam: inferences and geological significance. J. Metamorph. Geol. 28, 59-76.

Ngo, T. X., Santosh, M., Tran, H.T., Pham, H.T., 2015. Subduction initiation of Indochina and South China blocks: insight from the forearc ophiolitic peridotites of the Song Ma Suture Zone in Vietnam. Geol. J. 51(3), 421-442.

Nguyen, V.V., Hansen, B.,Wemmer, K., Lepvrier, C., Vu, V.T., Ta, T.T., 2013. U/Pb and Sm/Nd dating on ophiolitic rocks of the Song Ma suture zone (northern Vietnam): evidence for Upper Paleozoic Paleotethyan lithospheric remnants. J. Geodyn. 69, 140-147.

Pan, G., Chen, Z., Li, X., Xu, Q., Jiang, X., 1996. Models for the evolution of the polyarc-basin systems in eastern Tethys. Sediment. Facies Palaeogeogr. 16(2), 52-65. (in Chinese with English abstract)

Pham, T.H., Chen, F.K., Wang, W., Tam, B.M., Nguyen, T.B.T., Hoa, T.X., Li, X.H., 2008. Formation ages of granites and metabasalts in the Song Ma belt of northwestern Vietnam

and their tectonic implications. In: Conference Gondwana 13, Dali, China, Abstracts, 163.

Qi, X., Santosh, M., Zhu, L., Zhao, Y., Hu, Z., Zhang, C., Ji, F., 2014. Mid-Neoproterozoic arc magmatism in the northeastern margin of the Indochina block, SW China: geochronological and petrogenetic constraints and implications for Gondwana assembly. Precambrian Res. 245, 207-224.

Qi, X., Zeng, L., Zhu, L., Hu, Z., Hou, K., 2012. Zircon U-Pb and Lu-Hf isotopic systematics of the Daping plutonic rocks: implications for the Neoproterozoic tectonic evolution of the northeastern margin of the Indochina block, Southwest China. Gondwana Res. 21, 180-193.

Qian, X., Wang, Y., Zhang, Y., Zhang, Y., Senebouttalath, V., Zhang, A., He, H., 2019. Petrogenesis of the Permian-Triassic felsic igneous rocks along the Truong Son zone in northern Laos and their Paleotethyan assembly. Lithos 328-329, 101-114.

Qiu, L., Yan, D.-P., Yang, W.-X., Wang, J., Tang, X., Aviser, S. 2017. Early to Middle Triassic sedimentary records in the Youjiang Basin, South China: Implications for Indosinian orogenesis. J. Asian Earth Sci. 141, 125-139.

Richards, J.P., and Şengör, A.M.C., 2017. Did Paleo-Tethyan anoxia kill arc magma fertility for porphyry copper formation? Geology 45(7), 591-594.

Roger, F., Jolivet, M., Maluski, H., Respaut, J., Münch, P., Paquette, J., Vu Van, T., Nguyen Van, V., 2014. Emplacement and cooling of the Dien Bien Phu granitic complex: Implications for the tectonic evolution of the Dien Bien Phu Fault (Truong Son Belt, NW Vietnam). Gondwana Res. 26, 785-801.

Rossignol, C., Bourquin, S., Hallot, E., Poujol, M., Dabard, M.-P., Martini, R., Villeneuve, M., Cornee, J.J., Brayard, A., Roger, F., 2018. The Indosinian orogeny: A perspective from sedimentary archives of north Vietnam. J. Asian Earth Sci. 158, 352-380.

Sanematsu, K., Murakami, H., Duangsurigna, S., Vilayhack, S., Duncan, R.A., Watanabe, Y., 2011. $^{40}Ar/^{39}Ar$ ages of granitoids from the Truong Son fold belt and Kontum massif in Laos. J. Miner. Petrol. Sci. 106, 13-25.

Şengör, A.M.C., 1985. East Asian tectonic collage. Nature 318, 16-17.

Şengör, A.M.C., and Atayman, S., 2009, The Permian extinction and the Tethys: An exercise in global geology. Geological Society of America Special Paper 448, 96 p., doi: 10.1130/2009.2448.

Shao, T., Cheng, N., Song, M., 2016. Provenance and tectonic-paleogeographic evolution: Constraints from detrital zircon U–Pb ages of Late Triassic-Early Jurassic deposits in the

northern Sichuan basin, central China. J. Asian Earth Sci. 127, 12-31.

Shi, M.F., Lin, F.C., Fan, W.Y., Deng, Q., Cong, F., Tran, M.D., Zhu, H.P., Wang, H., 2015. Zircon U-Pb ages and geochemistry of granitoids in the Truong Son terrane, Vietnam: tectonic and metallogenic implications. J. Asian Earth Sci. 101, 101-120.

Sone, M., Metcalfe, I., 2008. Parallel Tethyan sutures in mainland Southeast Asia: New insights for Palaeo-Tethys closure and implications for the Indosinian orogeny. Compt. Rendus Geosci. 340, 166-179.

Stampfli, G.M., Borel, G.D., 2002. A plate tectonic model for the Paleozoic and Mesozoic constrained by dynamic plate boundaries and restored synthetic oceanic isochrons. Earth Planet. Sci. Lett. 196 (1-2), 17-33.

Tapponnier, P., Lacassin, R., Leloup, H., Scharer, U., Zhong, D., Liu, X., Ji, S., Zhang, L., Zhong, J., 1990. The Ailaoshan-Red river metamorphic belt: tertiary left-lateral shear between Indochina and South China. Nature 343, 431-437.

Thanh, X N., Santosh M., Hai TT., Hieu T P., 2016. Subduction initiation of Indochina and South China blocks: insight from the forearc ophiolitic peridotites of the Song Ma Suture Zone in Vietnam. Geol. J. 51, 421-442.

Tran, H.T., Zaw, Khin, Halpin, J.A., Manaka, T., Meffre, S., Lai, C., Lee, Y., Le, H.V., Dinh, S., 2014. The Tam Ky-Phuoc Son Shear Zone in central Vietnam: Tectonic and metallogenic implications. Gondwana Res. 26, 144-164.

Tran, T.H., Tran, T.A., Ngo, T.P., Pham, T.D., Tran, V.A., Izokh, A.E., Borisenko, A.S., Lan, C.Y., Chung, S.L., Lo, C.H., 2008. Permo-Triassic intermediate-felsic magmatism of the Truong Son belt, eastern margin of Indochina. Compt. Rendus Geosci. 340, 112-126.

Tran, V.T., Vu, K. (Eds.), 2011. Geology and Earth Resources of Vietnam 634. General Dept of Geology, and Minerals of Vietnam, Hanoi, Publishing House for Science and Technology, p. 634.

Trung, N., Tsujimori, T., Itaya, T., 2006. Honvang serpentinite body of the Song Ma fault zone, Northern Vietnam: a remnant of oceanic lithosphere within Indochina and South China suture. Gondwana Res. 9, 225-230.

Usuki, T., Lan, C.Y., Tran, T.H., Pham, T.D., Wang, K.L., Shellnutt, G.J., Chung, S.L., 2015. Zircon U-Pb ages and Hf isotopic compositions of alkaline silicic magmatic rocks in the Phan Si Pan-Tu Le region, northern Vietnam: Identification of a displaced western extension of the Emeishan Large Igneous Province. J. Asian Earth Sci. 97, 102-124.

Usuki, T., Lan, C.-Y., Wang, K.-L., Chiu, H.-Y., 2013. Linking the Indochina block and Gondwana during the early Paleozoic: evidence from U-Pb ages and Hf isotopes of

detrital zircons. Tectonophysics 586, 145-159.

van Achterbergh, E., Ryan, C., Jackson, S., Griffin, W.L., 2001. Appendix 3 data reduction software for LA-ICP-MS. In: Sylvester, P. (Ed.), Laser-Ablation-ICPMS in the Earth Sciences. Mineralogical Association of Canada, Short Courses, vol. 29. pp. 239-243.

Vermeesch, P., 2012. On the visualisation of detrital age distributions. Chem. GeoL. 312-313, 190-194.

Vượng, N.V., Hansen, B.T., Wemmer, K., Lepvrier, C., Tích, V.V., Thắng, T. T., 2013. U/Pb and Sm/Nd dating on ophiolitic rocks of the Song Ma suture zone (northern Vietnam): Evidence for upper paleozoic paleotethyan lithospheric remnants. J. Geodyn. 69, 140-147.

Wang, C., Liang, X., Foster, D.A., Fu, J., Jiang, Y., Dong, C., Zhou, Y., Wen, S., Quynh, P.V., 2016a. Detrital zircon U-Pb geochronology, Lu-Hf isotopes and REE geochemistry constrains on the provenance and tectonic setting of Indochina Block in the Paleozoic. Tectonophysics 677-678, 125-134.

Wang, C.Y., Zhou, M.F., Qi, L., 2007. Permian flood basalts and mafic intrusions in the Jinping (SW China)-Song Da (northern Vietnam) district: mantle sources, crustal contamination and sulfide segregation. Chem. Geol. 243, 317-343.

Wang, P.-L., Lo, C.-H., Chung, S.-L., Lee, T.-Y., Lan, C.-Y., Nam, T.N., Sano, Y., 2011. Thermochronology of the PoSen complex, northern Vietnam: implications for tectonic evolution in SE Asia. J. Asian Earth Sci. 40(5), 1044-1055.

Wang, Q., Deng, J., Li, C., Li, G., Yu, L., Qiao, L., 2014. The boundary between the Simao and Yangtze blocks and their locations in Gondwana and Rodinia: Constraints from detrital and inherited zircons. Gondwana Res. 26(2), 438-448.

Wang, S., Mo, Y., Wang, C., Ye, P., 2016b. Paleotethyan evolution of the Indochina Block as deduced from granites in northern Laos. Gondwana Res. 38, 183-196.

Wang, X.Y., Cao, D.H., Wang, Z.Q., Wang, A.J., Wu, Y.D., 2018. Zircon U-Pb age, trace element and Hf isotope composition of Sepon Au-Cu deposit, Laos: tectonic and metallogenic implications. China Geol. 1, 36-48.

Wang, Y., Lin, W., Faure, M., Lepvrier, C., Chu, Y., Nguyen, V.V., Hoai, L.T.T., Wei, W., Liu, F., Vu, T.V., 2021. Detrital zircon U-Pb age distribution and Hf isotopic constraints from the terrigenous sediments of the Song Chay Suture Zone (NE Vietnam) and their paleogeographic implications on the Eastern Paleo-Tethys evolution. Tectonics DOI: 10.1029/2020TC006611

Wang, Y., Qian, X., Cawood, P.A., Liu, H., Feng, Q., Zhao, G., Zhang, Y., He, H., Zhang, P., 2018. Closure of the East Paleotethyan Ocean and amalgamation of the Eastern Cimmerian and Southeast Asia continental fragments. Earth Sci. Rev. 186, 195-230.

Wang, Y., Wang, Y.J., Schoenbohm, L.M., Zhang, P., Zhang, B., Sobel, E.R., Zhou, R., Shi X., Zhang, J., Stockli, D.F., 2020. Cenozoic exhumation of the Ailaoshan-Red River shear zone: New insights from low-temperature thermochronology. Tectonics 39, e2020TC006151.

Wen, S., Yeh, Y.-L., Tang, C.-C., Phong, L.H., Toan, D.V., Chang, W.-Y., Chen, C.-H., 2015. The tectonic structure of the Song Ma fault zone, Vietnam. J. Asian Earth Sci. 107, 26-34.

Wu, F.Y., Wan, B., Zhao, L., Xiao, W.J., Zhu, R.X., 2020. Tethyan geodynamics. Acta Petrologic Sinica 36(6), 1627-1674.

Wu, F.Y., Yang, Y.H., Xie, L.W., Yang, J.H., Xu, P., 2006. Hf isotopic compositions of the standard zircons and baddeleyites used in U-Pb geochronology. Chem. Geol. 234, 105-126.

Xia, X., Nie, X., Lai, C.-K., Wang, Y., Long, X., Meffre, S., 2016. Where was the Ailaoshan Ocean and when did it open: A perspective based on detrital zircon U-Pb age and Hf isotope evidence. Gondwana Res. 36, 488-502.

Xia, X., Xu, J.; Huang, C., Long, X., Zhou, M., 2020.Subduction polarity of the Ailaoshan Ocean (eastern Paleotethys): Constraints from detrital zircon U-Pb and Hf-O isotopes for the Longtan Formation. Geol. Soc. Am. Bull. 132, 987-996.

Xiao, L, Xu, Y.G, Mei, H.J., He, B., Pirajno, F., 2004. Distinct mantle sources of low-Ti and high-Ti basalts from the western Emeishan large igneous province, SW China: implications for plume-lithosphere interaction. Earth Planet. Sci. Lett. 228, 525-546.

Xie, L., Zhang, Y., Zhang, H., Sun, J., Wu, F., 2008. In situ simultaneous determination of trace elements, U-Pb and Lu-Hf isotopes in zircon and baddeleyite. Sci. Bull. 53(10), 1565-1573.

Xu, J., Xia, X., Lai, C., Long, X., Huang, C., 2019. When Did the Paleotethys Ailaoshan Ocean Close: New Insights from Detrital Zircon U-Pb age and Hf Isotopes. Tectonics 38,1798-1823.

Xu, Y.G., Luo, Z.Y., Huang X.L., He B., Shi Y.R., He, B., Xiao, L., Xie, L.W., Shi, Y.R., 2008. Zircon U-Pb and Hf isotope constraints on crustal melting associated with the Emeishan mantle plume. Geochim. Cosmochim. Acta 72, 3084-3104.

Yang, J., Cawood, P.A., Du, Y., Huang, H., Hu, L., 2012. Detrital record of Indosinian mountain building in SW China: Provenance of the Middle Triassic turbidites in the Youjiang Basin. Tectonophysics 574-575, 105-117.

YNBGMR-Mojiang, 1976. Yunnan Bureau of Geological and Mineral Resources, Geological map of Mojiang region, scale 1: 200,000. China Ministry of Geology and Mineral Resource, Beijing (in Chinese).

Yumul, G.P., Zhou, M.F., Wang, Y.C., Zhao, T.P., Dimalanta, C.B., 2008. Geology and geochemistry of the Shuanggou ophiolite (Ailao Shan ophiolitic belt), Yunnan province, SW China: evidence for a slow-spreading oceanic basin origin. J. Asian Earth Sci. 32, 385-395.

Zhang, R.Y., Lo, C.H., Chung, S.L., Grove, M., Omori, S., Iizuka, Y., Liou, J.G., Tri, T.V., 2013. Origin and Tectonic Implication of Ophiolite and Eclogite in the Song Ma Suture Zone between the South China and Indochina Blocks. J. Metamorph. Geol. 31(1), 49-62.

Zhang, R.Y., Lo, C.H., Li, X.H., Chung, S.L., Anh, T.T., Tri, T.V., 2014. U-Pb dating and tectonic implication of ophiolite and metabasite from the Song Ma suture zone, Northern Vietnam. Am. J. Sci. 314, 649-678.

Zhang, X., Wang, Y., Clift, P.D., Yan, Y., Zhang, Y., Zhang, L., 2018. Paleozoic Tectonic Setting and Paleogeographic Evolution of the Qin-Fang Region, Southern South China Block: Detrital Zircon U-Pb Geochronological and Hf Isotopic Constraints. Geochemistry, Geophysics, Geosystems 19(10), 3962-3979.

Zhong, D., 1998. The Paleotethys orogenic belt in west of Sichuan and Yunnan. Beijing: Science Publishing House. (in Chinese)

Zhong, N., Song, X., Xu, H., Jiang, H., 2017. Influence of a tectonically active mountain belt on its foreland basin. Evidence from detrital zircon dating of bedrocks and sediments from the eastern Tibetan Plateau and Sichuan Basin, SW China. J. Asian Earth Sci. 146, 251-264.

Zhou, X., Yu, J.-H., O'Reilly, S.Y., Griffin, W.L., Sun, T., Wang, X., Tran, M.D., Nguyen, D.L., 2018. Component variation in the late Neoproterozoic to Cambrian sedimentary rocks of SW China - NE Vietnam, and its tectonic significance. Precambrian Res. 308, 92-110.

Zhu, M., 2016. The depositional record of Southwestern Upper Yangtze area during Triassic and its restriction on the tectonic framework of basin and range. Doctor thesis, Zhejiang University. (in Chinese with English abstract)

Zi, J.W., Cawood, P.A., Fan, W.M., Wang, Y.J., Tohver, E., McCuaig, T.C., Peng, T.P., 2012. Triassic collision in the Paleo-Tethys Ocean constrained by volcanic activity in SW China. Lithos 144-145, 145-160.

Table 1 facies and interpretation of the analyzed samples from the Ailaoshan-Song Ma mélange and its adjacent active margin in IB

	Sample number	GPS location	Lithofacies	Description	Depositional environment	Tectonic setting	Geochronological constraints
M1	TH05	19.79065° N, 105.51487° E	Schistosed medium to fine grained sandstone	Dark grey to grey grain supported sandstone with medium grain size, the framework detritus is angular shaped, and in low sphericity, schistocity well developed	Non-Smith strata, matrix of a serpentinite block	Song Ma ophiolitic mélange unit	Song Ma formation, *Inouya* sp.? Indicated as Cambrian strata. Being the matrix of a serpentinite block, a late Carboniferous to middle Triassic age was suggested
	AS103	23.4469° N, 101.8703° E	Sericite schist (meta-sandstone)	Elongated quartz and newly formed muscovite formed the foliation of the schist	Wall rock of a serpentinite block	Ailaoshan Ophiolitic mélange unit	No report
	AS147	23.6550° N, 101.6337° E	Schistosed fine grained sandstone from interbedding series	Dark yellow to grey fine grained sandstone interbedded with pelite layer, the sandstone	Non-Smith strata, matrix of a serpentinite block	Ailaoshan Ophiolitic mélange unit	No report

			of fine grained sandstone and pelite	is grain supported, the framework detritus is subangular and in low sphericity, the layer of the sandstone is 30-50 cm in thickness while the layer of pelite is 50-100 cm in thickness. highly sheared			
	TH03	19.60914° N, 105.71722° E	Pelite and siltstone	Yellow to grey pelite and siltstone	Non-Smith strata, matrix of a serpentinite block	Song Ma ophiolitic mélange unit	Song Ma formation, *Inouya* sp.? Indicated as Cambrian strata. Being the matrix of a serpentinite block, a late Carboniferous to middle Triassic was suggested
M3	TH11	19.86216° N, 105.41061° E	Schisted tuff with very thin interbedded pelite	cryptocrystalline, the strata of tuff is normally 10-30 cm in thickness, highly sheared	Non-Smith strata, matrix of a serpentinite block	Ophiolitic mélange unit	Ditto
	TH12	19.86482° N, 105.44180° E	Schisted sandstone	Dark grey coarse to medium grained, highly	Non-Smith strata, matrix of a serpentinite block	Ophiolitic mélange unit	Ditto

				sheared			
	AS79	23.4175° N, 101.6768° E	laminated medium to fine grained sandstone	Light grey to grey fine grained sandstone which is about 10 cm in thickness interbedded with millimetric to centimetric mudstone layers, well sorted and roundness, representing the DE of Bouma sequence	semi deep-sea environment	Sedimentary cover of IB, Nilaoshan belt	*Pristiograptus regularis Tornquist, Monograptus priodon (Bronn), Monoclimacis cf. vomerinus*
IB North margin	TH09	19.73538° N, 105.45736° E	medium to fine grained sandstone	Purplish red fine grained sandstone, 50-100 cm in thickness, interbedded with mudstone	Shallow-marine environment	Forearc basin of Truong Son belt	Dong Trau formation, *Neoschizodus ovatus elongatus, Costatoria proharpa.*
	TH13	19.88329° N, 105.29522° E	Thick bedded cross-laminated sandstone	Purplish red coarse grained sandstone which is 50-100 cm in thickness, with the presence of muscovite and	Shallow-marine environment	Forearc basin of Truong Son belt	Indicated as the Silurian strata. According to our work, P-T strata were suggested

			volcanic debris			
TH14	19.88328° N, 105.30289° E	Cross-laminated sandstone	Purplish red coarse grained sandstone, with the presence of muscovite and volcanic debris	Shallow-marine environment	Forearc basin of Truong Son belt	Indicated as the Silurian strata. According to our work, (middle) Triassic strata was suggested
TH01	19.56466° N, 105.71004° E	Massive sandstone	Grey coarse grained massive sandstone without deformation and metamorphism	Littoral or lacustrine environment	Post-orogenic intra-continental sediments	Dong Do formation, *Yalina*(?) sp., *Cycadites saladini*

Table 2 Summary of the four measures of youngest age of detrital zircon grains in our analyzed samples

	sample	YSG	YPP	YC1σ (2+) [a]	YC2σ (3+) [a]
M1	**TH05**	**263.3±2.2**	**439**	**370.4±2.6 (2)**	**435.6±3.7 (17)**
	AS103	**371.4±3.9**	**432**	**435.5±4.6 (12)**	**435.5±4.6 (12)**
	AS147	**373.7±3.8**	**425**	**436.4±4.6 (6)**	**428.6±4.5 (8)**
	YN-54	427.2±6.7	440	441.5±6.0 (9)	449.2±6.6 (11)
	YN-41	399.7±5.1	440	401.3±4.7 (2)	435.1±5.5 (15)
M2	AE02	229±4.6	250	259.8±3.2 (3)	254.6±2.8

					(5)
	AW06	261.5±2.47	460	444.3±5.9 (2)	450.1±5.5 (3)
	AW07	239±2.2	260	258.3±2.9 (18)	257.3±2.8 (19)
	AW08	242±2.8	260	260.0±2.7 (39)	259.5±2.7 (41)
	AW10	232.4±2.4	260	258.3±2.[illegible] (7)	258.3±2.5 (7)
M3	AW17	237±3	245	2[illegible]3.3±2.5 (47)	244.2±2.5 (49)
	AW20	236±3	245	244.9±2.4 (29)	244.9±2.4 (29)
	13YZ06	236±2	245	246.9±2.4 (31)	246.9±2.4 (31)
	TH03	**223.2±11.0**	**240**	**242.6±6.2 (20)**	**242.6±6.2 (20)**
	TH11	**217.0±21.3**	**247**	**249.3±6.7 (99)**	**249.3±6.7 (99)**
	TH12	**224.4±4.8**	**245**	**244.7±4.8 (69)**	**244.7±4.8 (69)**
IB North	**AS79**	**425.5±4.4**	**440**	**441.1±4.6 (13)**	**441.1±4.6 (13)**
	TH09	**232.0±6.9**	**260**	**257.0±6.0 (14)**	**257.0±6.0**

margin					**(14)**
	TH13	**225.6±2.1**	**269**	**270.6±3.4 (76)**	**270.6±3.4 (76)**
	TH14	**223.8±3.1**	**245**	**242.6±2.6 (22)**	**246.3±3.8 (25)**
	TH01	**217.3±6.2**	**240**	**247.0±4.4 (31)**	**248.1±4.5 (34)**

Notes to Table: YSG: youngest single grain age; YPP: youngest graphical age peak; YC1σ (2+): youngest 1σ grain cluster; YC2σ (3+): youngest 2σ grain cluster. [a]Numbers of grain ages in clusters in parentheses.

Table 3 Summary of the characteristic of M1, M2 and M3 unit

Mélange unit	Samples	Tectonic locations	Detrital age spectrum	Youngest age	Phanerozoic zircon $\varepsilon_{Hf}(t)$ value	T_{DM}^2	Speculative sources
M1	**AS103**, **AS147**, **TH05**, YN41, YN54	Middle segment of Ailaoshan ophiolitic mélange and part of SE Song Ma ophiolitic mélange	**435 Ma**, 810 Ma, **970 Ma**, 1085 Ma, 1690 Ma, 1860 Ma, 2510 Ma	263.3±2.2	-19.6 ~ +10.2 with peak at **-8.0**	Peaks at 1.55 Ga, **2.05 Ga**, 2.35 Ga, 2.95 Ga	1. Main Paleozoic sedimentary cover (especially Silurian sedimentary rocks) in **IB**; 2. Very small amount from magmatic rocks in the ophiolitic mélange.
M2	AW02, AW06, AW07, AW08, AW10	NW segment of Ailaoshan ophiolitic mélange	**260 Ma**, **410 Ma**, 770 Ma, 950 Ma, 1840 Ma, 2480 Ma	229±4.6	-28 ~ +8 with peaks at -10.5, -2.5, **+0.4**, +5.0	Peaks at **0.85 Ga**, 1.55 Ga, 1.75 Ga, 1.95 Ga	1. Dominant from ELIP and related rocks in **SCB**; 2. Very small amount from recycled the

						sedimentary rocks in **IB**.
M3	**TH03**, **TH11**, **TH12**, AW17, AW20, 13YZ06	SE segment of Ailaoshan ophiolitic mélange and Song Ma ophiolitic mélange	**245 Ma**, 360 Ma, 770 Ma, 1045 Ma	224.4±4.8	-26 ~ +12 with peaks at **-8**, +2.2	Peaks at 1.05 Ga, **1.45 Ga**	1. Dominant from Magmatic arc in **IB** (WALS-Truong Son belt); 2. Very small amount from southwest margin of the **SCB**.

Notes to Table: the bold sample is from this study, the rest from Xia et al. (2016, 2020) and Xu et al. (2019). In the detrital age spectrum, the bold ages represent the major age peaks

Fig. 1 Tectonic map of Asia showing the main microcontinents of SE Asia and Tibet with emphasis on the Ailaoshan- Song Ma suture zone between South China and Indochina or Sibumasu blocks respectively (Faure et al., 2016). RRF: Red River Fault, SCF: Song Chay Fault; DBF: Dien Bien Phu Fault; WAl:Western Ailaoshan zone; ALSZ: Ailaoshan suture zone; JP: Jinping basalt; SC: Song Chay massif; SCSZ: Song Chay suture zone; SMSZ: Song Ma suture zone; SD: Song Da.

Fig. 2 Geological map of Ailaoshan (adapted from 1:20000 geological map of Yunnan) with the sample locations (blue marks are the samples of this study, black marks are from Xu et al. (2019), Xia et al. (2020))

Fig. 3 Geological map of the Thanh Hoa area (adapted from the 1:20000 geological map of Vietnam) with the locations of analyzed sample.

Fig. 4 Simplified granitoids distribution map of West Ailaoshan-Truong Son belt (adapted from Hou et al., 2019) with the age distritution pattern inserted. RRF: Red River Fault, SCF: Song Ca Fault; SMF: Song Ma fault; DBF: Dien Bien Phu fault.

Fig. 5 Representative outcrop photos of the analyzed samples. A. AS79, Silurian laminated sandstone interbedded with mudstone layers. Sedimentary cover of the Indochina Block, Ailaoshan area. B. AS103, sericite schist, matrix of a serpentinite block, Ailaoshan area. C. AS147, Schistose sandstone-mudstone alternations, matrix of a serpentinite block, Ailaoshan area. D. TH01, Late Triassic (T3) coarse grained sandstone, interpreted as molasse formation, Thanh Hoa area. E. TH03, Pelite and siltstone, matrix of a serpentinite block, Thanh Hoa area.

Fig. 5 Representative outcrop photos of the analyzed samples. F. TH05, Schistosed medium to fine grained sandstone, matrix of a serpentinite block, Thanh Hoa area. G. TH09, Middle Triassic (T2) purplish red fine grained sandstone, interbedded with mudstone, sedimentary rocks of the North margin of ICB, Thanh Hoa area. H. TH11, Schistosed tuff with very thin interbedded pelite, matrix of a serpentinite block, Thanh Hoa area. I. TH12, schistosed sandstone, matrix of a serpentinite block, Thanh Hoa area. J. TH13, coarse sandstone with cross bedding, sedimentary rocks of the North margin of ICB, Thanh Hoa area.

Fig. 6 Microphotographs showing the textural features and mineral compositions of the analyzed samples from Ailaoshan-Song Ma ophiolitic mélange. A. gravel-size quartz and rock fragments in the fine grain matrix in AS79; B. oriented muscovite and elongated quartz indicating a pervasive shearing in AS103; C. Moderate sorted, angular to sub-angular quartz and lithic fragments in AS147; D. undeformed and poorly sorted quartz and lithic fragments in TH01; E. extra-fine-grained quartz and muscovite in TH03; F. poorly sorted, angular quartz in TH05; G. poorly sorted, angular to subangular quartz and lithic fragments in TH09.H. elongated quartz and oriented muscovite that define the well-developed foliation in TH11;

Fig. 7 Representative cathodoluminescence (CL) images of selected detrital zircons from the Ailaoshan-Song Ma ophiolitic mélange. The red and yellow circles represent U-Pb and Lu-Hf

isotopic analytical sites, respectively. The red and yellow numbers represent U-Pb age, ε_{Hf} (t) values and T_{DM}^2 , respectively.

Fig. 8 Kernel Density Estimate diagrams of U/Pb ages of the detrital zircons from the AilaoshanSong Ma ophiolitic mélange. See Figs. 2 and 3 for sample locations, and Table S1 for zircon ages

Fig. 9 Diagrams of T_{DM}^2 values from the same samples as those analyzed for detrital zircons in the Ailaoshan-Song Ma ophiolitic mélange.

Fig. 10 A. Temporal variations of εHf(t) values at 0-3.0 Ga of this study. The crustal evolution range comes from Linnemann et al. (2014). Dashed lines demonstrate evolution of zircons with depleted mantle model ages between 1.0 Ga, 1.9 Ga and 2.5 Ga. Half of the analyzed zircons plot in the crustal evolution zone between 1.0 Ga and 1.9 Ga, but Archean data are consistent with the range of the Archean crust. B. Diagram of the two-stage model Hf age (T_{DM}^2) versus age plots for detrital zircons, indicating the source of zircons. Zircon Hf model ages are older than their crystallization ages, revealing a formation from re-melting of older crustal rocks crystallized during the previous events.

Fig. 11 Synthetic and comparison of the cumulative probability plots of detrital zircon U-Pb ages from the different units (M1, M2, and M3) Ailaoshan-Song Ma ophiolitic mélange (this study, Xia et al., 2016, 2020; and Xu et al., 2019).

Fig. 12 Diagrams of T_{DM}^2 values from the samples as those analyzed for detrital zircons in the different units (M1, M2, and M3) of the Ailaoshan-Song Ma ophiolitic mélange (this study, Xia et al., 2016, 2020; and Xu et al., 2019), and ELIP (Xu et al., 2008; Usuki et al., 2015)

Fig. 13 Temporal variations of εHf (t) values at 0-3.0 Ga of all the measurement of the Ailaoshan-Song Ma ophiolitic mélange with the separation of M1 (This study, Xia et al., 2016), M2 (Xia et al., 2020), M3 (Xu et al., 2019) and ELIP (Xu et al., 2008; Usuki et al., 2015).

Fig. 14 Synthetic and comparison of the cumulative probability plots of detrital zircon U-Pb ages from the Ailaoshan-Song Ma (This study, Xia et al., 2016, 2020; and Xu et al., 2019) and Song Chay ophiolitic mélanges (Wang et al., under review).

Fig. 15 Synthesis and comparison of Kernel Density Estimate diagrams of detrital zircon U-Pb ages. Cathaysia block including the region of Qin-Fang (Zhang et al., 2018), Shiwandashan (Hu et al., 2014, 2015, 2017) and Youjiang basins (Yang et al., 2012; Duan et al., 2017; Qiu et al., 2017); Western margin of SCB (Longmenshan) (Shao et al., 2015; Chen et al., 2016, 2018; Zhong et al., 2017; Zhu et al., 2016); SW margin of the SCB (NE region of Ailaoshan belt) (Xia et al., 2016, 2020; Xu et al., 2019); NW part of Indochina block (Simao area) (Xia et al., 2016, 2020; Xu et al., 2019); Central Indochina block (Truong Son and Sam Nua belt) (Wang et al., 2016; Rossignol et al., 2018).

Fig. 16 Temporal variations of ε_{Hf} (t) and T_{DM}^{2} values between 200-300 Ma of all the measurement of the West Ailaoshan-Truong Son magmatic belt with the separation of Early stage (A1), Late stage (A2), Emeishan large igneous province (ELIP), and post orogenic magmatism (PO).

Fig. 17 Schematic reconstruction of the Late Carboniferous-Middle Triassic geodynamic evolution between the SCB and IB to illustrate the provenance of detrital zircon in different units along the Ailaoshan-Song Ma suture zone.

Fig. 18 Palaeogeographic reconstructions for Eastern Paleo-Tethys of the Late Car□boniferous-Middle Triassic between the SCB and IB based on the provenance of the detrital zircon from the Ailaoshan-Song Ma ophiolite (Adapted from Metcafe, 2013; Dong et al, 2021). NCB: North China Block. SCB: South China Block; NQTB: North Qiangtang Block; SQTB: South Qiangtang Block; IB: Indochina Block.

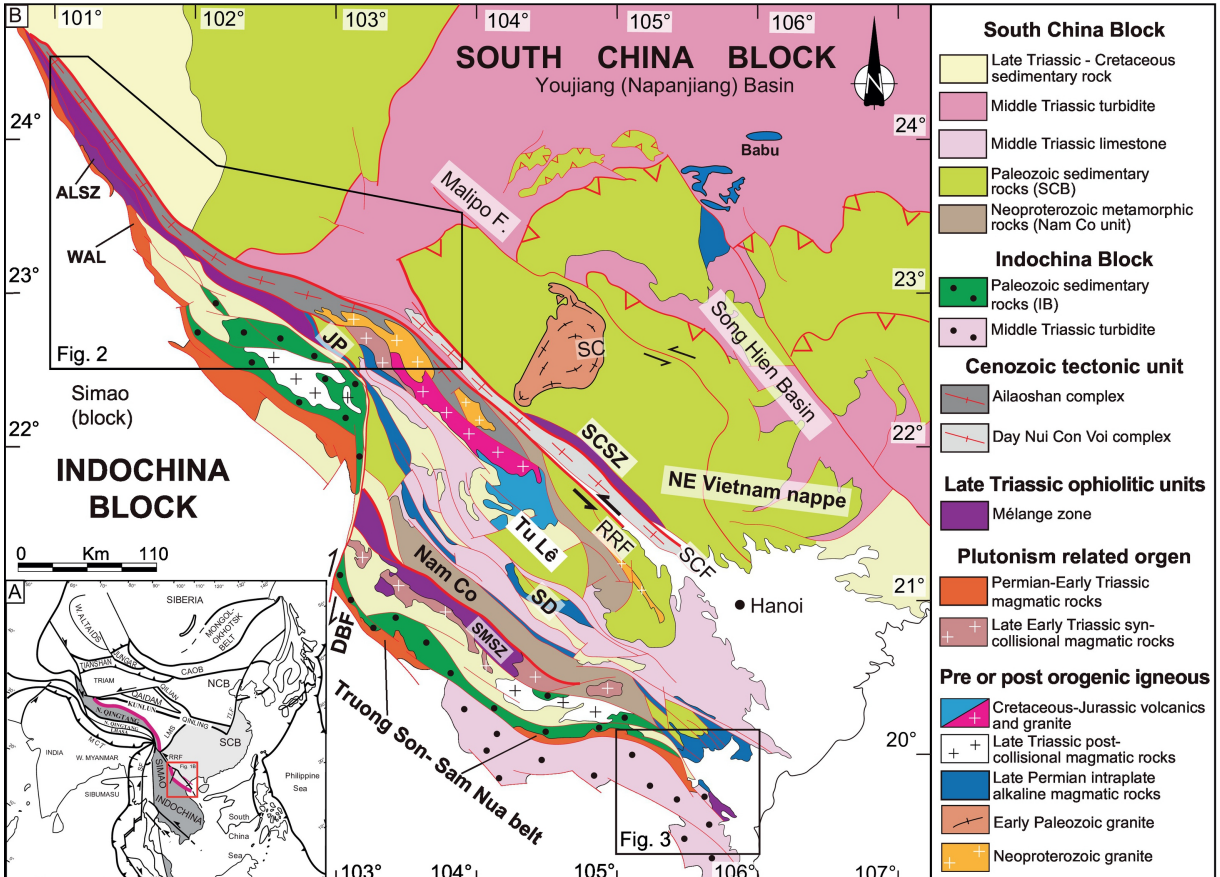
B
101°
102°
103°
104°
105°
106°
SOUTH CHINA BLOCK
Youjiang (Napanjiang) Basin
24°
23°
22°
21°
20°
ALSZ
WAL
Fig. 2
Simao
(block)
INDOCHINA
BLOCK
Malipo F.
Babu
JP
SC
Song Hien Basin
SCSZ
NE Vietnam nappe
Tu Lê
RRF
SCF
Nam Co
SD
SMSZ
DBF
Truong Son- Sam Nua belt
Hanoi
Fig. 3
0 Km 110
A
SIBERIA
INDIA
W. MYANMAR
SUMATRA
SIBUMASU
Philippine Sea
South China Sea
SCB
NCB
CAOB
INDOCHINA
South China Block
Late Triassic - Cretaceous sedimentary rock
Middle Triassic turbidite
Middle Triassic limestone
Paleozoic sedimentary rocks (SCB)
Neoproterozoic metamorphic rocks (Nam Co unit)
Indochina Block
Paleozoic sedimentary rocks (IB)
Middle Triassic turbidite
Cenozoic tectonic unit
Ailaoshan complex
Day Nui Con Voi complex
Late Triassic ophiolitic units
Mélange zone
Plutonism related orgen
Permian-Early Triassic magmatic rocks
Late Early Triassic syn-collisional magmatic rocks
Pre or post orogenic igneous
Cretaceous-Jurassic volcanics and granite
Late Triassic post-collisional magmatic rocks
Late Permian intraplate alkaline magmatic rocks
Early Paleozoic granite
Neoproterozoic granite

Figure 1

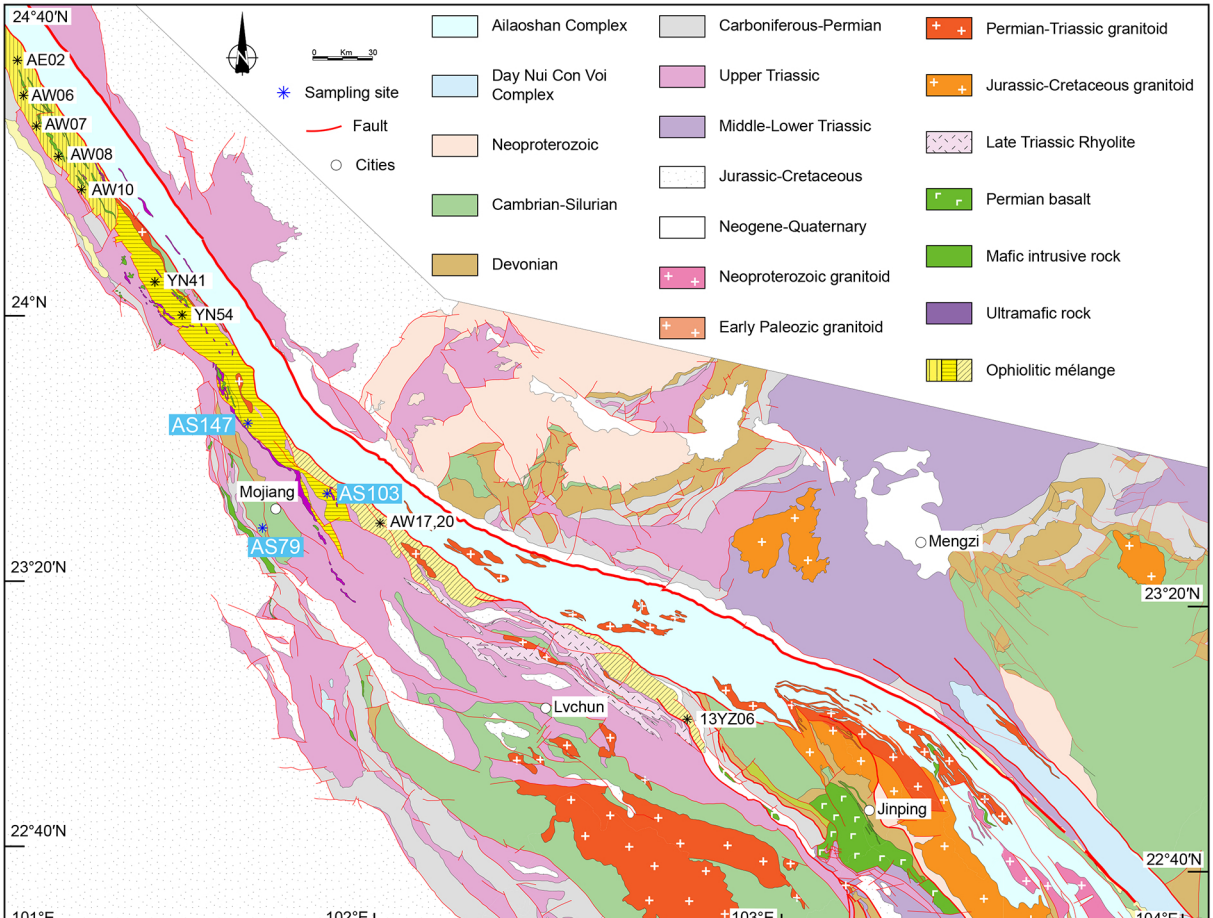
24°40'N
AE02
AW06
AW07
AW08
AW10
YN41
YN54
24°N
AS147
Mojiang
AS103
AW17,20
AS79
23°20'N
Lvchun
13YZ06
Mengzi
23°20'N
Jinping
22°40'N
22°40'N
101°E
102°E
103°E
104°E
0 Km 30
Sampling site
Fault
Cities
Ailaoshan Complex
Day Nui Con Voi Complex
Neoproterozoic
Cambrian-Silurian
Devonian
Carboniferous-Permian
Upper Triassic
Middle-Lower Triassic
Jurassic-Cretaceous
Neogene-Quaternary
Neoproterozoic granitoid
Early Paleozic granitoid
Permian-Triassic granitoid
Jurassic-Cretaceous granitoid
Late Triassic Rhyolite
Permian basalt
Mafic intrusive rock
Ultramafic rock
Ophiolitic mélange

Figure 2

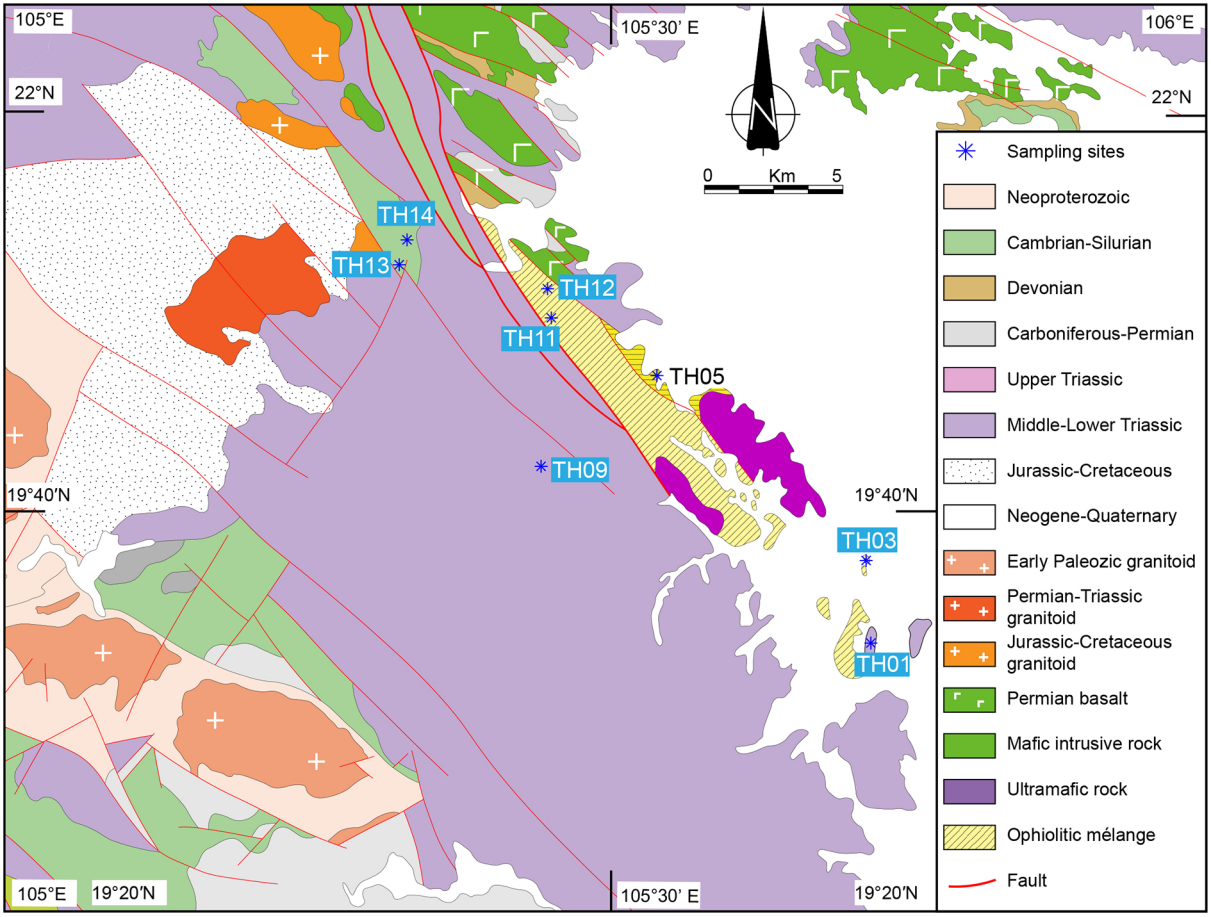
105°E
22°N
105°30' E
106°E
22°N
N
0 Km 5
TH14
TH13
TH12
TH11
TH05
TH09
TH03
TH01
19°40'N
19°40'N
105°E
19°20'N
105°30' E
19°20'N
Sampling sites
Neoproterozoic
Cambrian-Silurian
Devonian
Carboniferous-Permian
Upper Triassic
Middle-Lower Triassic
Jurassic-Cretaceous
Neogene-Quaternary
Early Paleozic granitoid
Permian-Triassic granitoid
Jurassic-Cretaceous granitoid
Permian basalt
Mafic intrusive rock
Ultramafic rock
Ophiolitic mélange
Fault

Figure 3

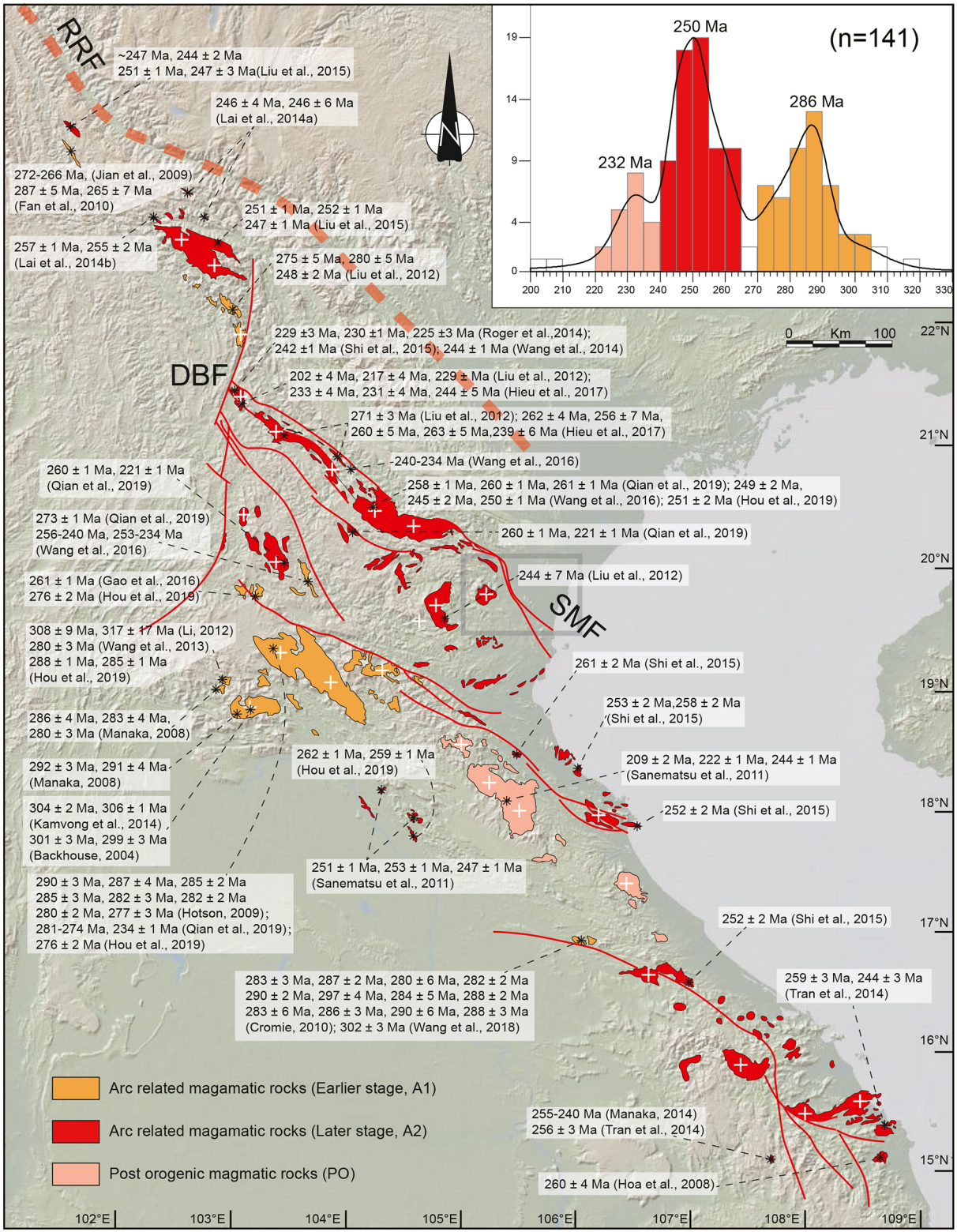
RRF
DBF
SMF
~247 Ma, 244 ± 2 Ma
251 ± 1 Ma, 247 ± 3 Ma(Liu et al., 2015)
246 ± 4 Ma, 246 ± 6 Ma
(Lai et al., 2014a)
272-266 Ma, (Jian et al., 2009)
287 ± 5 Ma, 265 ± 7 Ma
(Fan et al., 2010)
251 ± 1 Ma, 252 ± 1 Ma
247 ± 1 Ma (Liu et al., 2015)
257 ± 1 Ma, 255 ± 2 Ma
(Lai et al., 2014b)
275 ± 5 Ma, 280 ± 5 Ma
248 ± 2 Ma (Liu et al., 2012)
229 ±3 Ma, 230 ±1 Ma, 225 ±3 Ma (Roger et al.,2014);
242 ±1 Ma (Shi et al., 2015); 244 ± 1 Ma (Wang et al., 2014)
202 ± 4 Ma, 217 ± 4 Ma, 229 ± Ma (Liu et al., 2012);
233 ± 4 Ma, 231 ± 4 Ma, 244 ± 5 Ma (Hieu et al., 2017)
271 ± 3 Ma (Liu et al., 2012); 262 ± 4 Ma, 256 ± 7 Ma,
260 ± 5 Ma, 263 ± 5 Ma,239 ± 6 Ma (Hieu et al., 2017)
240-234 Ma (Wang et al., 2016)
260 ± 1 Ma, 221 ± 1 Ma
(Qian et al., 2019)
258 ± 1 Ma, 260 ± 1 Ma, 261 ± 1 Ma (Qian et al., 2019); 249 ± 2 Ma,
245 ± 2 Ma, 250 ± 1 Ma (Wang et al., 2016); 251 ± 2 Ma (Hou et al., 2019)
273 ± 1 Ma (Qian et al., 2019)
256-240 Ma, 253-234 Ma
(Wang et al., 2016)
260 ± 1 Ma, 221 ± 1 Ma (Qian et al., 2019)
261 ± 1 Ma (Gao et al., 2016)
276 ± 2 Ma (Hou et al., 2019)
244 ± 7 Ma (Liu et al., 2012)
308 ± 9 Ma, 317 ± 17 Ma (Li, 2012)
280 ± 3 Ma (Wang et al., 2013)
288 ± 1 Ma, 285 ± 1 Ma
(Hou et al., 2019)
261 ± 2 Ma (Shi et al., 2015)
253 ± 2 Ma,258 ± 2 Ma
(Shi et al., 2015)
286 ± 4 Ma, 283 ± 4 Ma,
280 ± 3 Ma (Manaka, 2008)
262 ± 1 Ma, 259 ± 1 Ma
(Hou et al., 2019)
209 ± 2 Ma, 222 ± 1 Ma, 244 ± 1 Ma
(Sanematsu et al., 2011)
292 ± 3 Ma, 291 ± 4 Ma
(Manaka, 2008)
304 ± 2 Ma, 306 ± 1 Ma
(Kamvong et al., 2014)
301 ± 3 Ma, 299 ± 3 Ma
(Backhouse, 2004)
252 ± 2 Ma (Shi et al., 2015)
251 ± 1 Ma, 253 ± 1 Ma, 247 ± 1 Ma
(Sanematsu et al., 2011)
290 ± 3 Ma, 287 ± 4 Ma, 285 ± 2 Ma
285 ± 3 Ma, 282 ± 3 Ma, 282 ± 2 Ma
280 ± 2 Ma, 277 ± 3 Ma (Hotson, 2009);
281-274 Ma, 234 ± 1 Ma (Qian et al., 2019);
276 ± 2 Ma (Hou et al., 2019)
252 ± 2 Ma (Shi et al., 2015)
283 ± 3 Ma, 287 ± 2 Ma, 280 ± 6 Ma, 282 ± 2 Ma
290 ± 2 Ma, 297 ± 4 Ma, 284 ± 5 Ma, 288 ± 2 Ma
283 ± 6 Ma, 286 ± 3 Ma, 290 ± 6 Ma, 288 ± 3 Ma
(Cromie, 2010); 302 ± 3 Ma (Wang et al., 2018)
259 ± 3 Ma, 244 ± 3 Ma
(Tran et al., 2014)
255-240 Ma (Manaka, 2014)
256 ± 3 Ma (Tran et al., 2014)
260 ± 4 Ma (Hoa et al., 2008)
250 Ma
286 Ma
232 Ma
(n=141)
0 Km 100
Arc related magamatic rocks (Earlier stage, A1)
Arc related magamatic rocks (Later stage, A2)
Post orogenic magmatic rocks (PO)
22°N
21°N
20°N
19°N
18°N
17°N
16°N
15°N
102°E
103°E
104°E
105°E
106°E
107°E
108°E
109°E

Figure 4

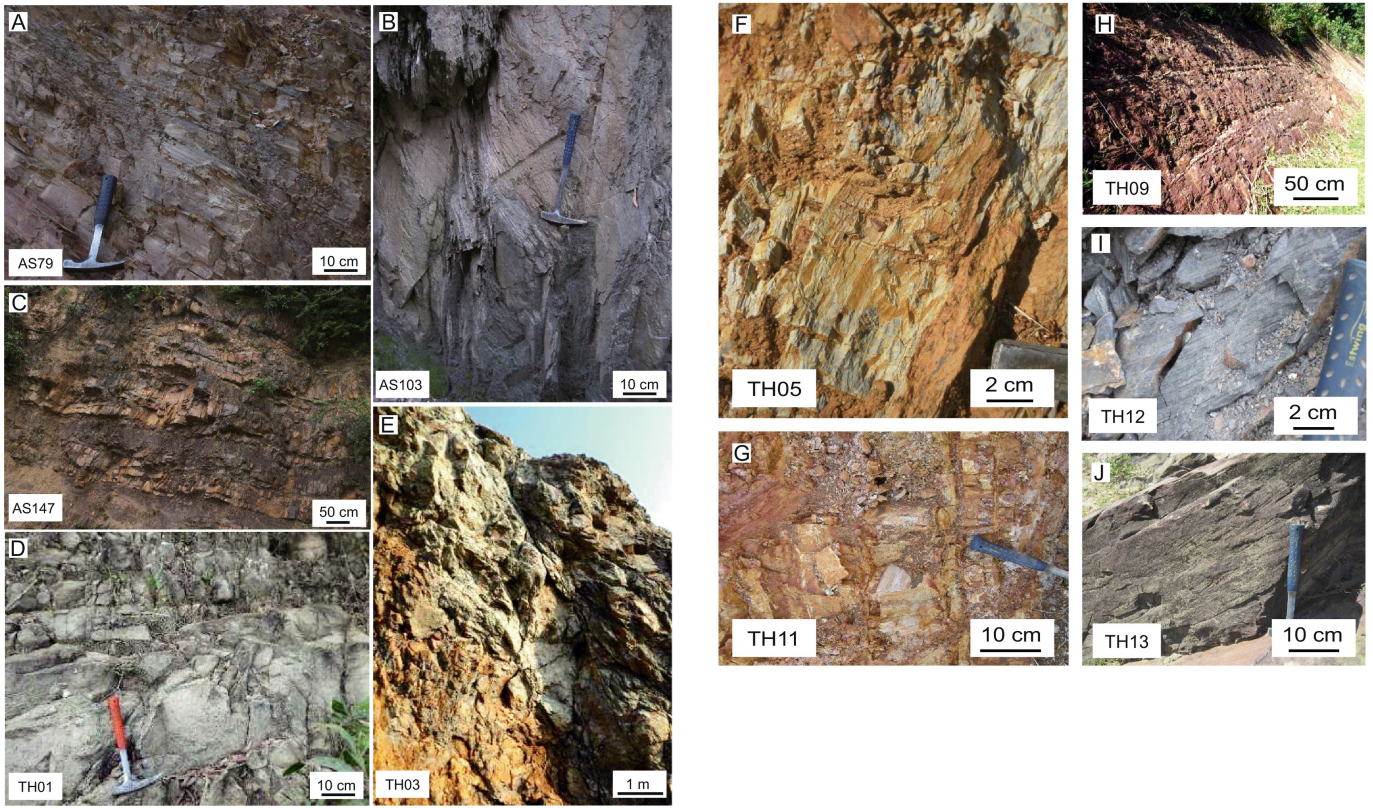
A
AS79
10 cm
B
AS103
10 cm
C
AS147
50 cm
D
TH01
10 cm
E
TH03
1 m
F
TH05
2 cm
G
TH11
10 cm
H
TH09
50 cm
I
TH12
2 cm
J
TH13
10 cm

Figure 5

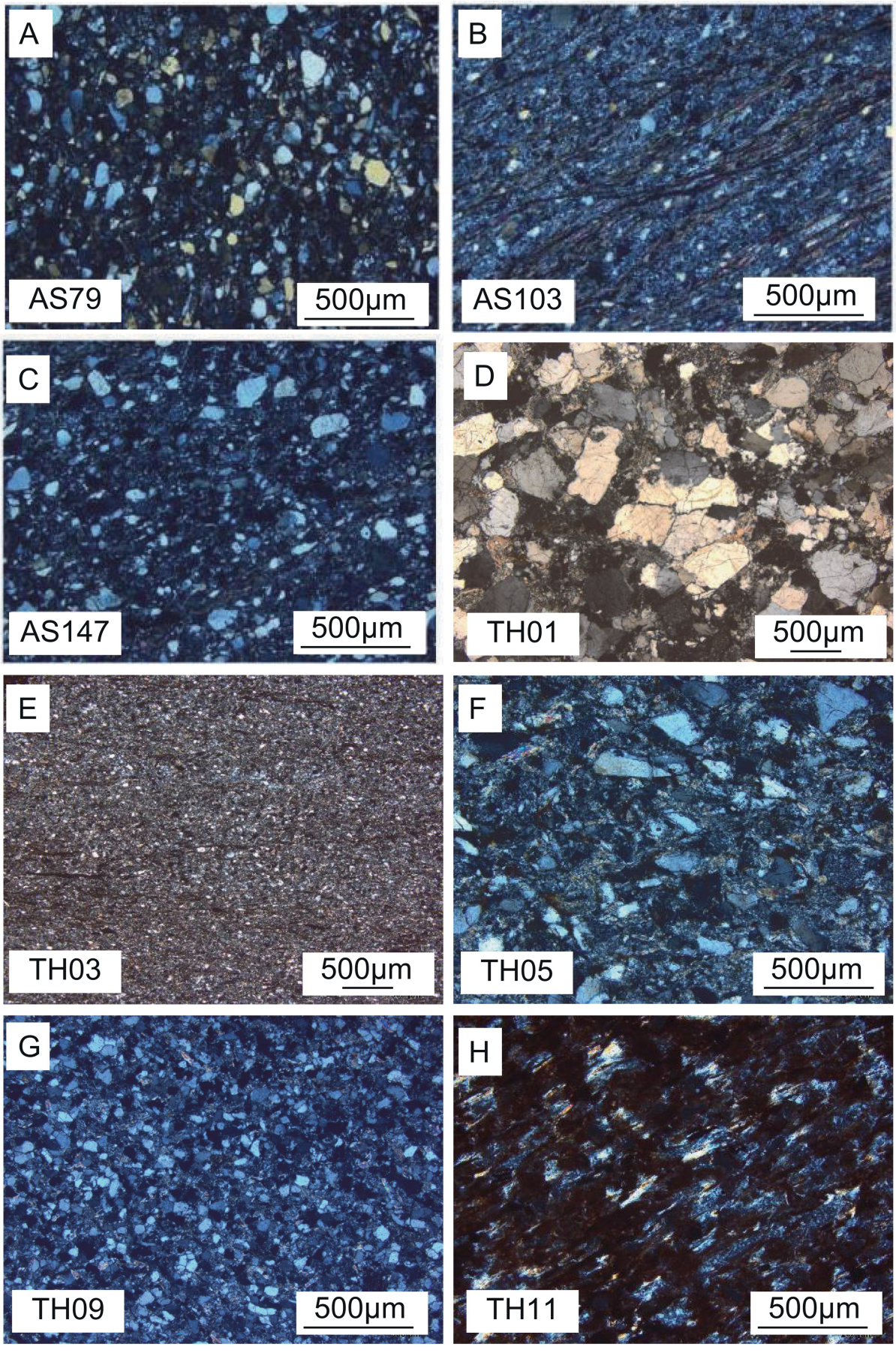
A
AS79
500µm
B
AS103
500µm
C
AS147
500µm
D
TH01
500µm
E
TH03
500µm
F
TH05
500µm
G
TH09
500µm
H
TH11
500µm

Figure 6

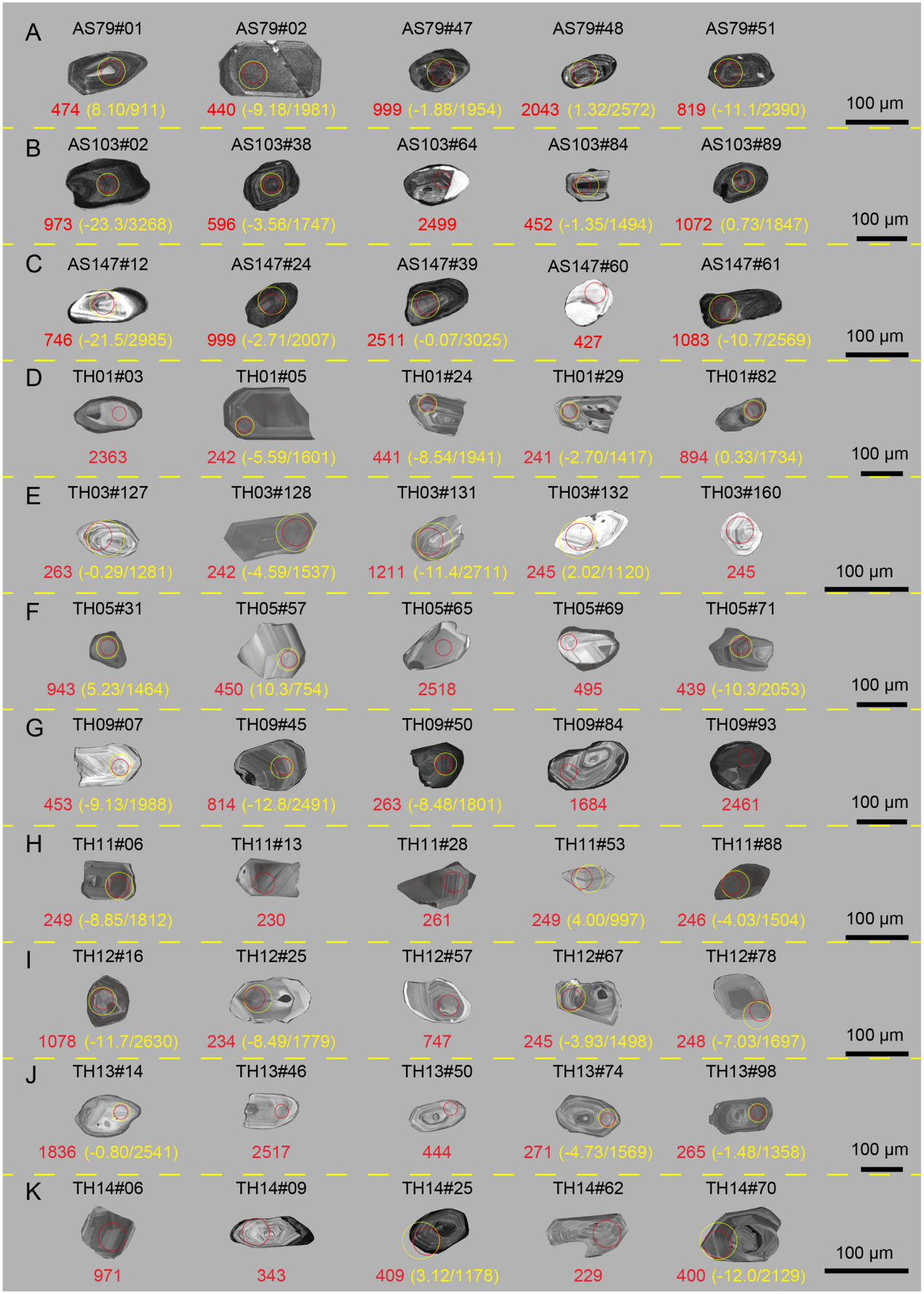
A
AS79#01
AS79#02
AS79#47
AS79#48
AS79#51
474 (8.10/911)
440 (-9.18/1981)
999 (-1.88/1954)
2043 (1.32/2572)
819 (-11.1/2390)
100 µm
B
AS103#02
AS103#38
AS103#64
AS103#84
AS103#89
973 (-23.3/3268)
596 (-3.56/1747)
2499
452 (-1.35/1494)
1072 (0.73/1847)
100 µm
C
AS147#12
AS147#24
AS147#39
AS147#60
AS147#61
746 (-21.5/2985)
999 (-2.71/2007)
2511 (-0.07/3025)
427
1083 (-10.7/2569)
100 µm
D
TH01#03
TH01#05
TH01#24
TH01#29
TH01#82
2363
242 (-5.59/1601)
441 (-8.54/1941)
241 (-2.70/1417)
894 (0.33/1734)
100 µm
E
TH03#127
TH03#128
TH03#131
TH03#132
TH03#160
263 (-0.29/1281)
242 (-4.59/1537)
1211 (-11.4/2711)
245 (2.02/1120)
245
100 µm
F
TH05#31
TH05#57
TH05#65
TH05#69
TH05#71
943 (5.23/1464)
450 (10.3/754)
2518
495
439 (-10.3/2053)
100 µm
G
TH09#07
TH09#45
TH09#50
TH09#84
TH09#93
453 (-9.13/1988)
814 (-12.8/2491)
263 (-8.48/1801)
1684
2461
100 µm
H
TH11#06
TH11#13
TH11#28
TH11#53
TH11#88
249 (-8.85/1812)
230
261
249 (4.00/997)
246 (-4.03/1504)
100 µm
I
TH12#16
TH12#25
TH12#57
TH12#67
TH12#78
1078 (-11.7/2630)
234 (-8.49/1779)
747
245 (-3.93/1498)
248 (-7.03/1697)
100 µm
J
TH13#14
TH13#46
TH13#50
TH13#74
TH13#98
1836 (-0.80/2541)
2517
444
271 (-4.73/1569)
265 (-1.48/1358)
100 µm
K
TH14#06
TH14#09
TH14#25
TH14#62
TH14#70
971
343
409 (3.12/1178)
229
400 (-12.0/2129)
100 µm

Figure 7

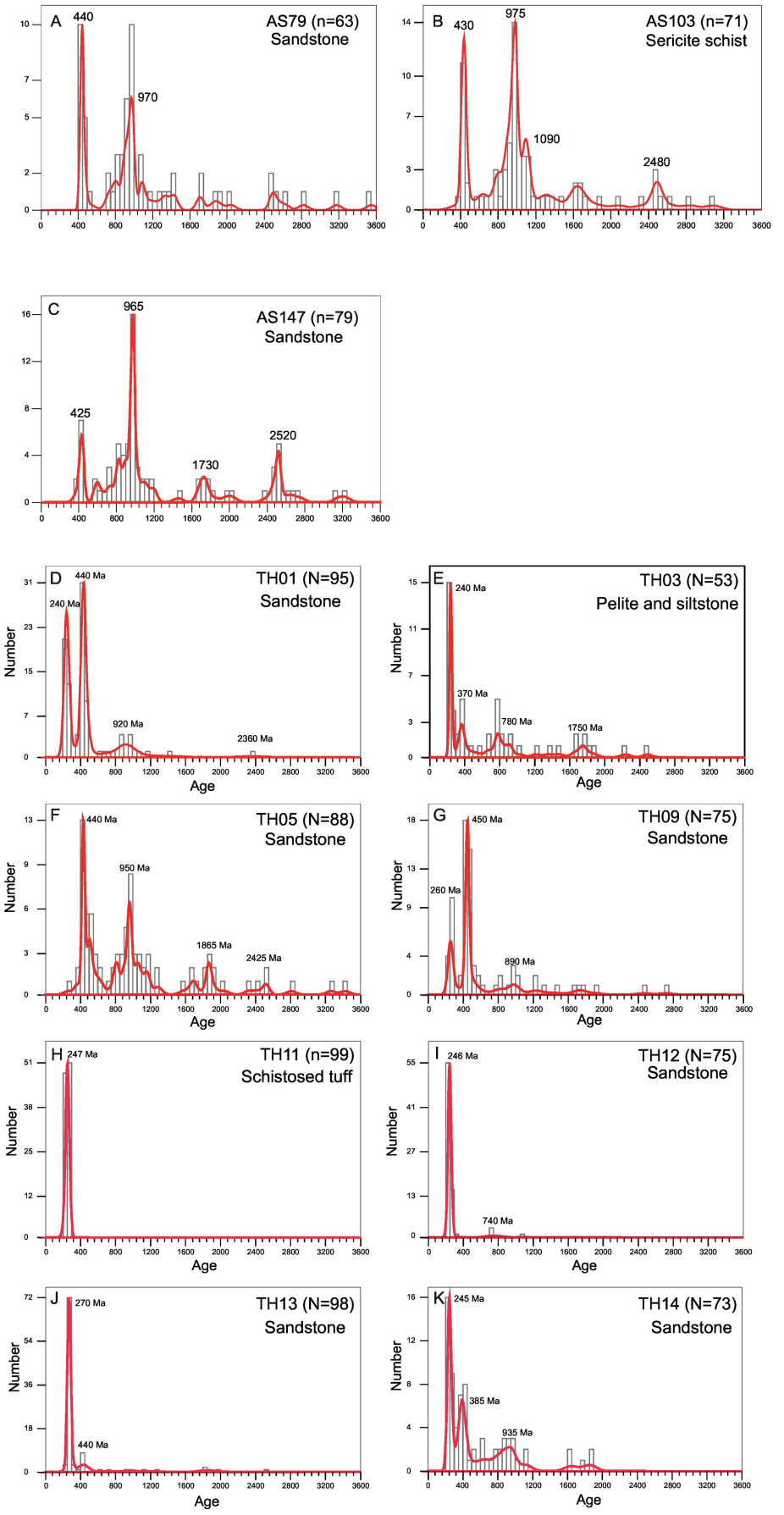
A
440
970
AS79 (n=63)
Sandstone
B
430
975
1090
2480
AS103 (n=71)
Sericite schist
C
425
965
1730
2520
AS147 (n=79)
Sandstone
D
440 Ma
240 Ma
920 Ma
2360 Ma
TH01 (N=95)
Sandstone
E
240 Ma
370 Ma
780 Ma
1750 Ma
TH03 (N=53)
Pelite and siltstone
F
440 Ma
950 Ma
1865 Ma
2425 Ma
TH05 (N=88)
Sandstone
G
450 Ma
260 Ma
890 Ma
TH09 (N=75)
Sandstone
H
247 Ma
TH11 (n=99)
Schistosed tuff
I
246 Ma
740 Ma
TH12 (N=75)
Sandstone
J
270 Ma
440 Ma
TH13 (N=98)
Sandstone
K
245 Ma
385 Ma
935 Ma
TH14 (N=73)
Sandstone
Number
Age

Figure 8

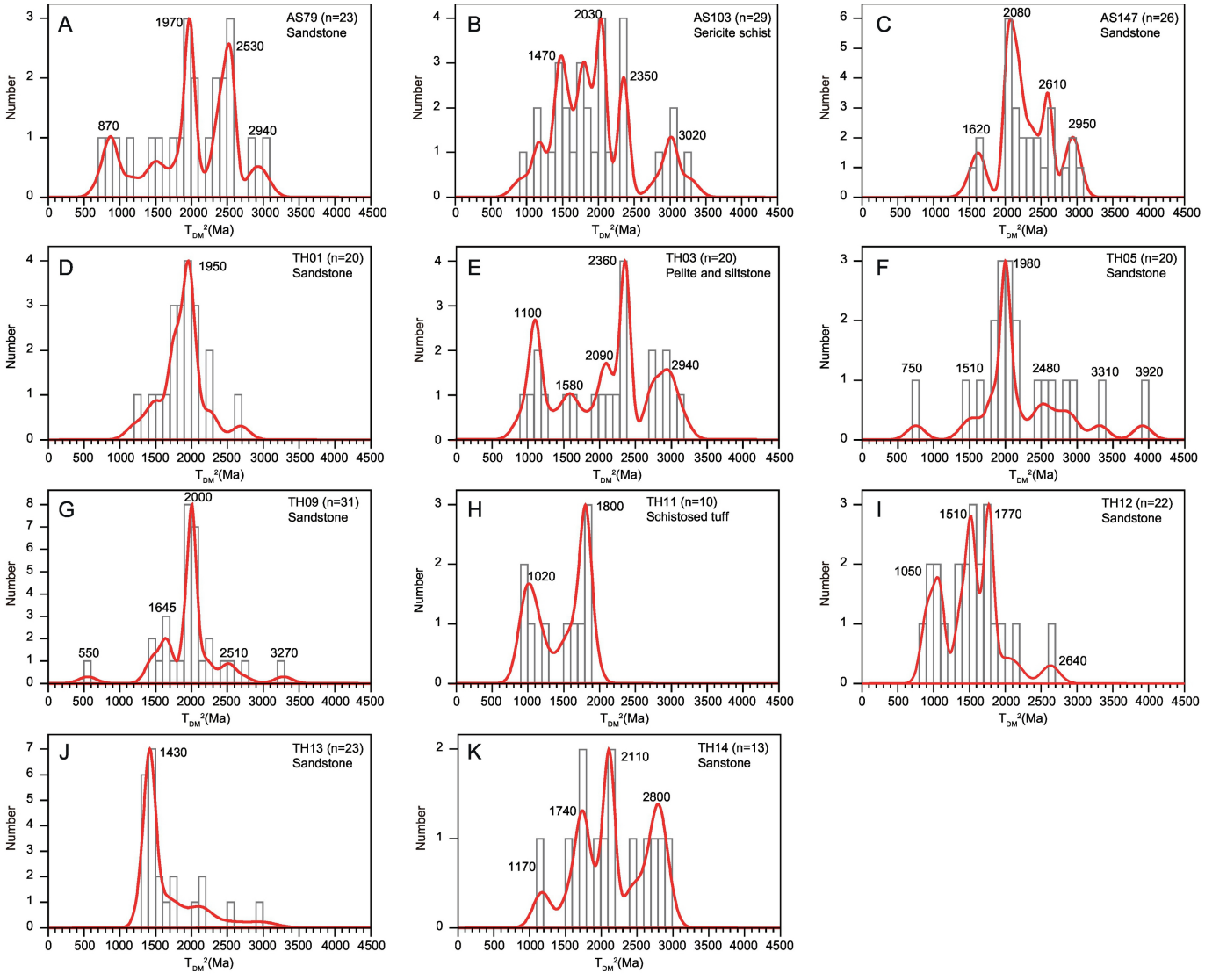
A
AS79 (n=23)
Sandstone
870
1970
2530
2940
B
AS103 (n=29)
Sericite schist
1470
2030
2350
3020
C
AS147 (n=26)
Sandstone
1620
2080
2610
2950
D
TH01 (n=20)
Sandstone
1950
E
TH03 (n=20)
Pelite and siltstone
1100
1580
2090
2360
2940
F
TH05 (n=20)
Sandstone
750
1510
1980
2480
3310
3920
G
TH09 (n=31)
Sandstone
550
1645
2000
2510
3270
H
TH11 (n=10)
Schistosed tuff
1020
1800
I
TH12 (n=22)
Sandstone
1050
1510
1770
2640
J
TH13 (n=23)
Sandstone
1430
K
TH14 (n=13)
Sanstone
1170
1740
2110
2800
Number
T_{DM}^2(Ma)

Figure 9

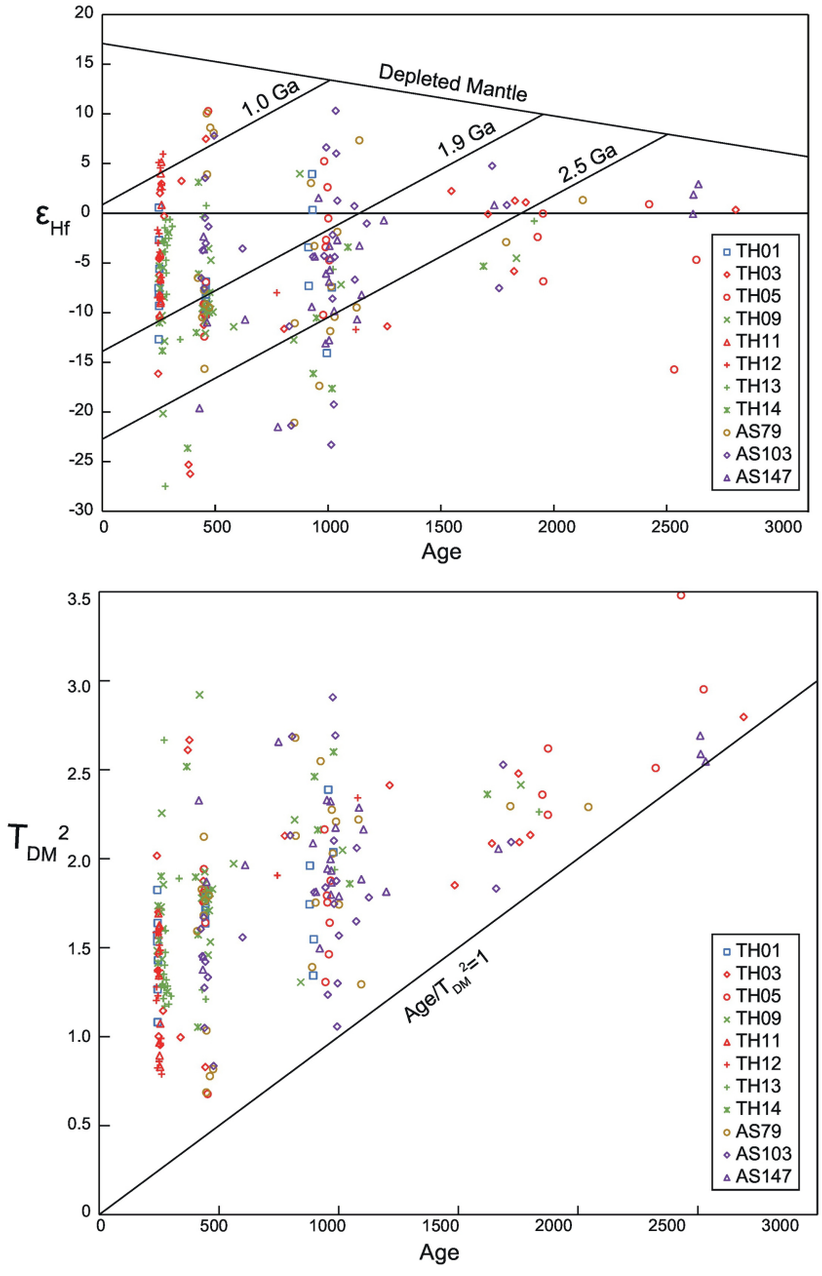
Depleted Mantle
1.0 Ga
1.9 Ga
2.5 Ga
εHf
Age
TH01
TH03
TH05
TH09
TH11
TH12
TH13
TH14
AS79
AS103
AS147
TDM2
Age/TDM2=1

Figure 10

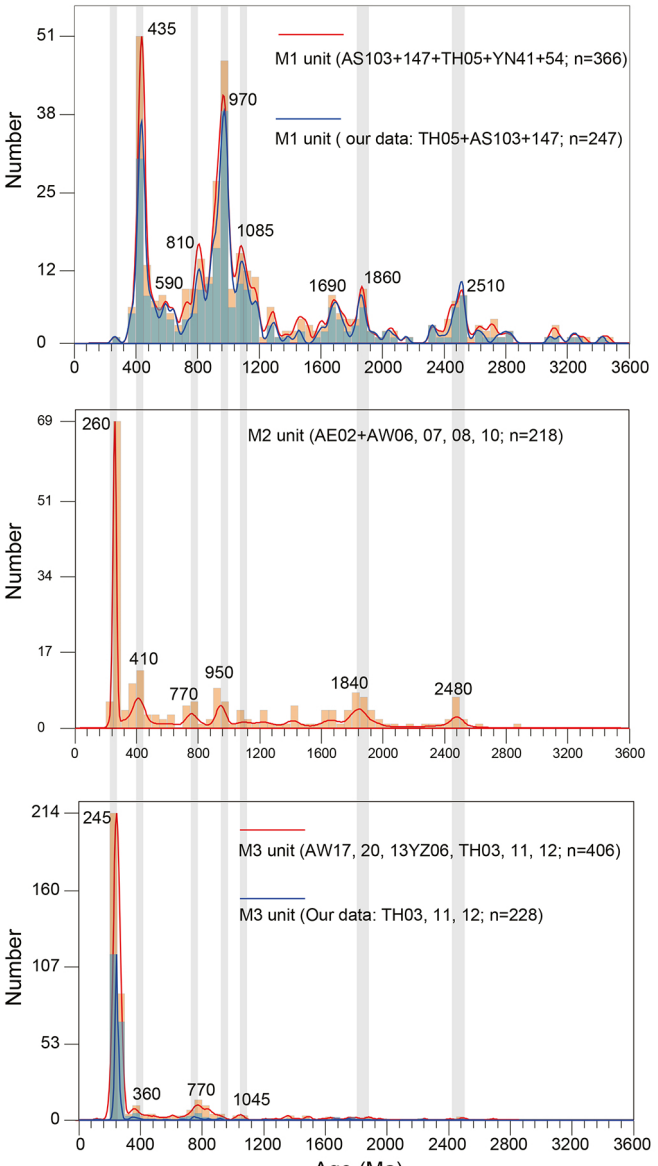
M1 unit (AS103+147+TH05+YN41+54; n=366)
M1 unit (our data: TH05+AS103+147; n=247)
435
970
810
1085
590
1690
1860
2510
M2 unit (AE02+AW06, 07, 08, 10; n=218)
260
410
770
950
1840
2480
M3 unit (AW17, 20, 13YZ06, TH03, 11, 12; n=406)
M3 unit (Our data: TH03, 11, 12; n=228)
245
360
770
1045
Number
Age (Ma)

Figure 11

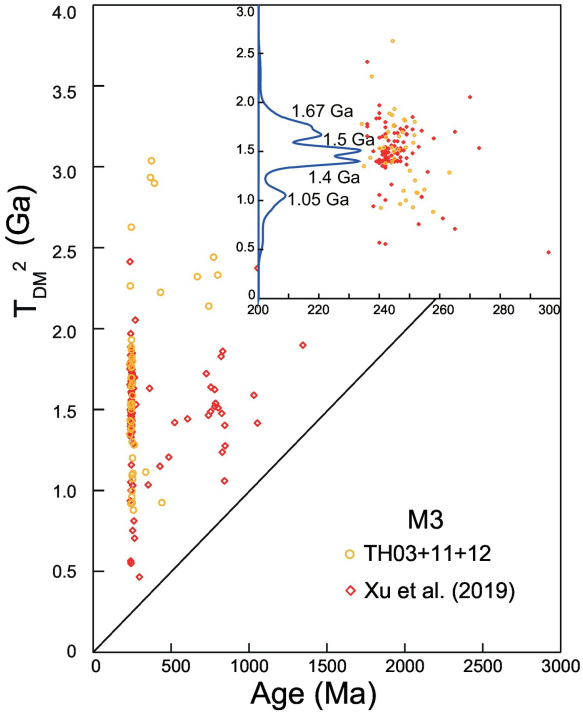
1.67 Ga
1.5 Ga
1.4 Ga
1.05 Ga
M3
TH03+11+12
Xu et al. (2019)
T_{DM}^2 (Ga)
Age (Ma)

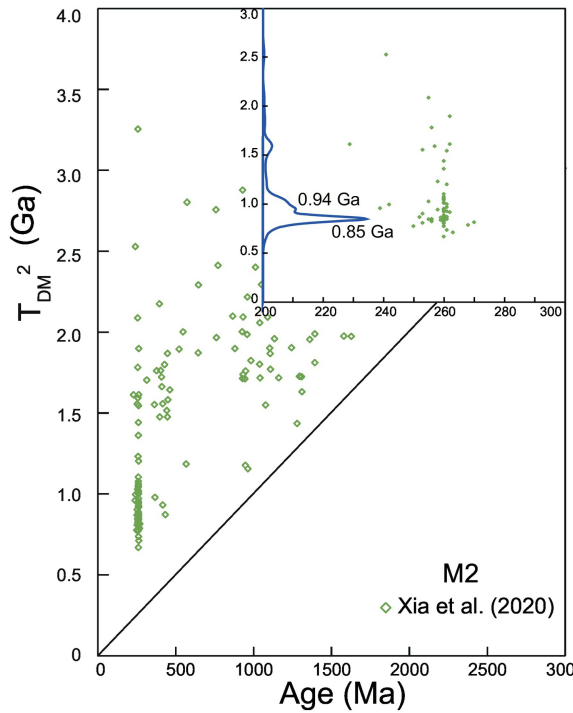
0.94 Ga
0.85 Ga
M2
Xia et al. (2020)
T_{DM}^2 (Ga)
Age (Ma)

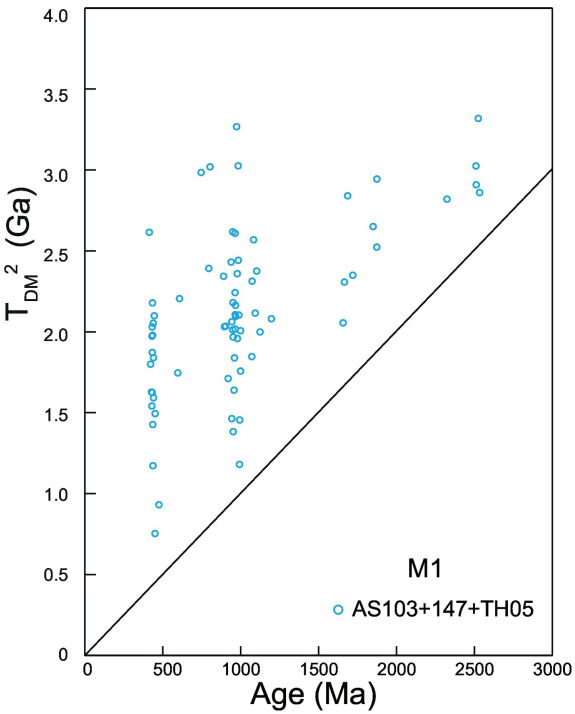
M1
AS103+147+TH05
T_{DM}^2 (Ga)
Age (Ma)

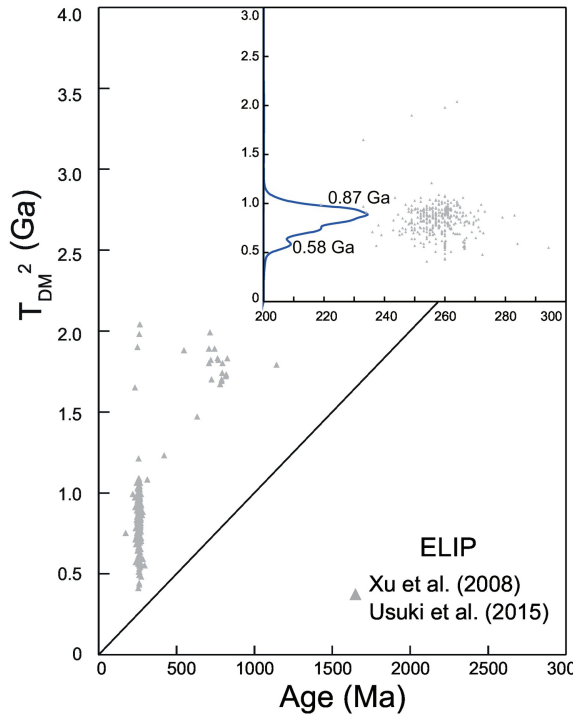
0.87 Ga
0.58 Ga
ELIP
Xu et al. (2008)
Usuki et al. (2015)
T_{DM}^2 (Ga)
Age (Ma)

Figure 12

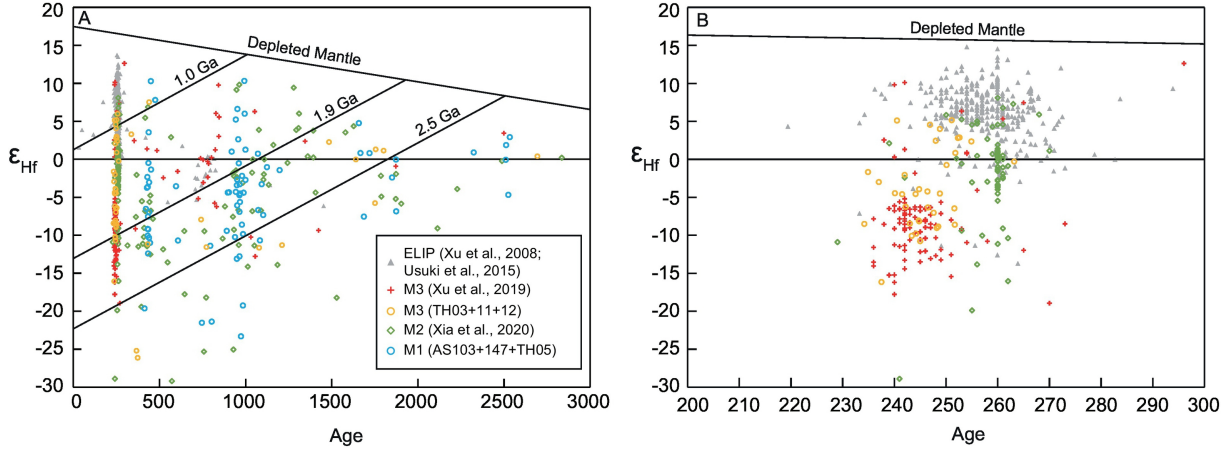
A
B
Depleted Mantle
1.0 Ga
1.9 Ga
2.5 Ga
ε_{Hf}
Age
ELIP (Xu et al., 2008; Usuki et al., 2015)
M3 (Xu et al., 2019)
M3 (TH03+11+12)
M2 (Xia et al., 2020)
M1 (AS103+147+TH05)

Figure 13

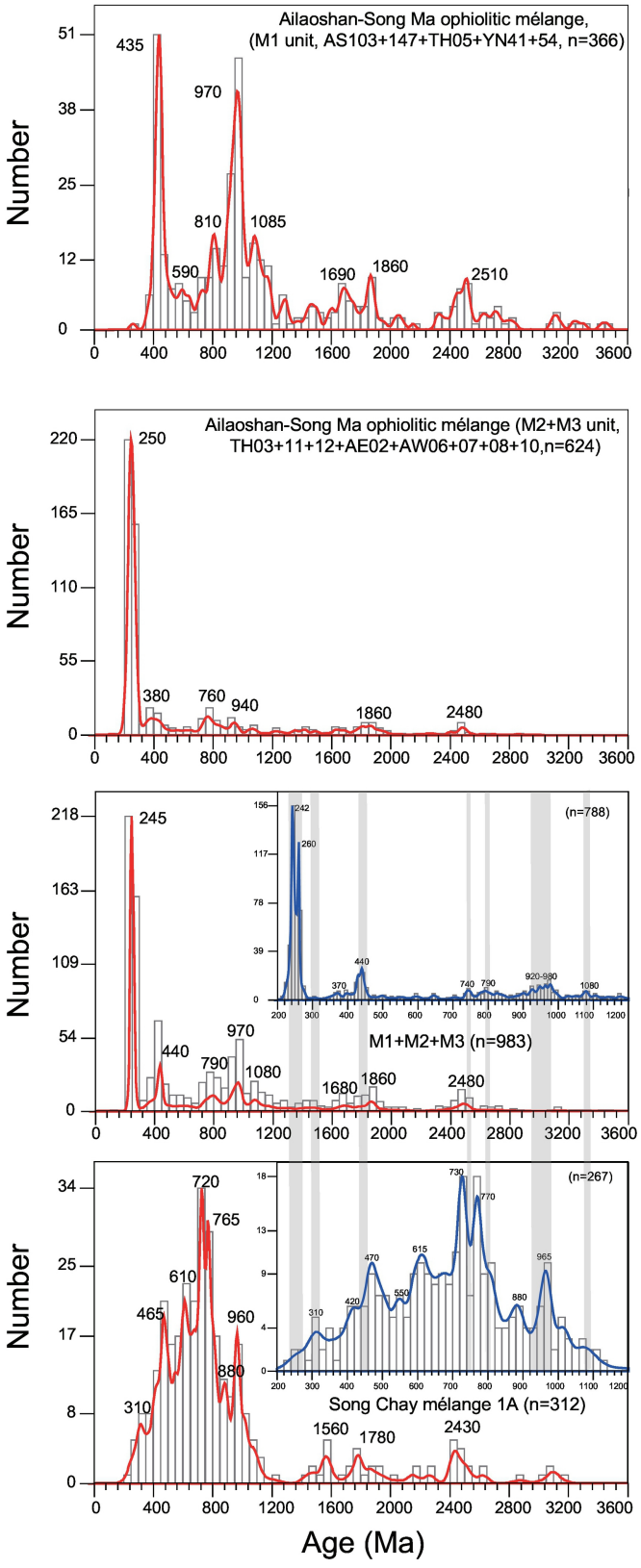
Ailaoshan-Song Ma ophiolitic mélange,
(M1 unit, AS103+147+TH05+YN41+54, n=366)
435
970
810
1085
590
1690
1860
2510
Number
Ailaoshan-Song Ma ophiolitic mélange (M2+M3 unit,
TH03+11+12+AE02+AW06+07+08+10,n=624)
250
380
760
940
1860
2480
Number
245
242
260
(n=788)
440
370
740
790
920-980
1080
M1+M2+M3 (n=983)
970
440
790
1080
1680
1860
2480
Number
720
765
610
465
960
880
310
730
770
470
615
965
420
550
880
310
Song Chay mélange 1A (n=312)
1560
1780
2430
Number
Age (Ma)

Figure 14

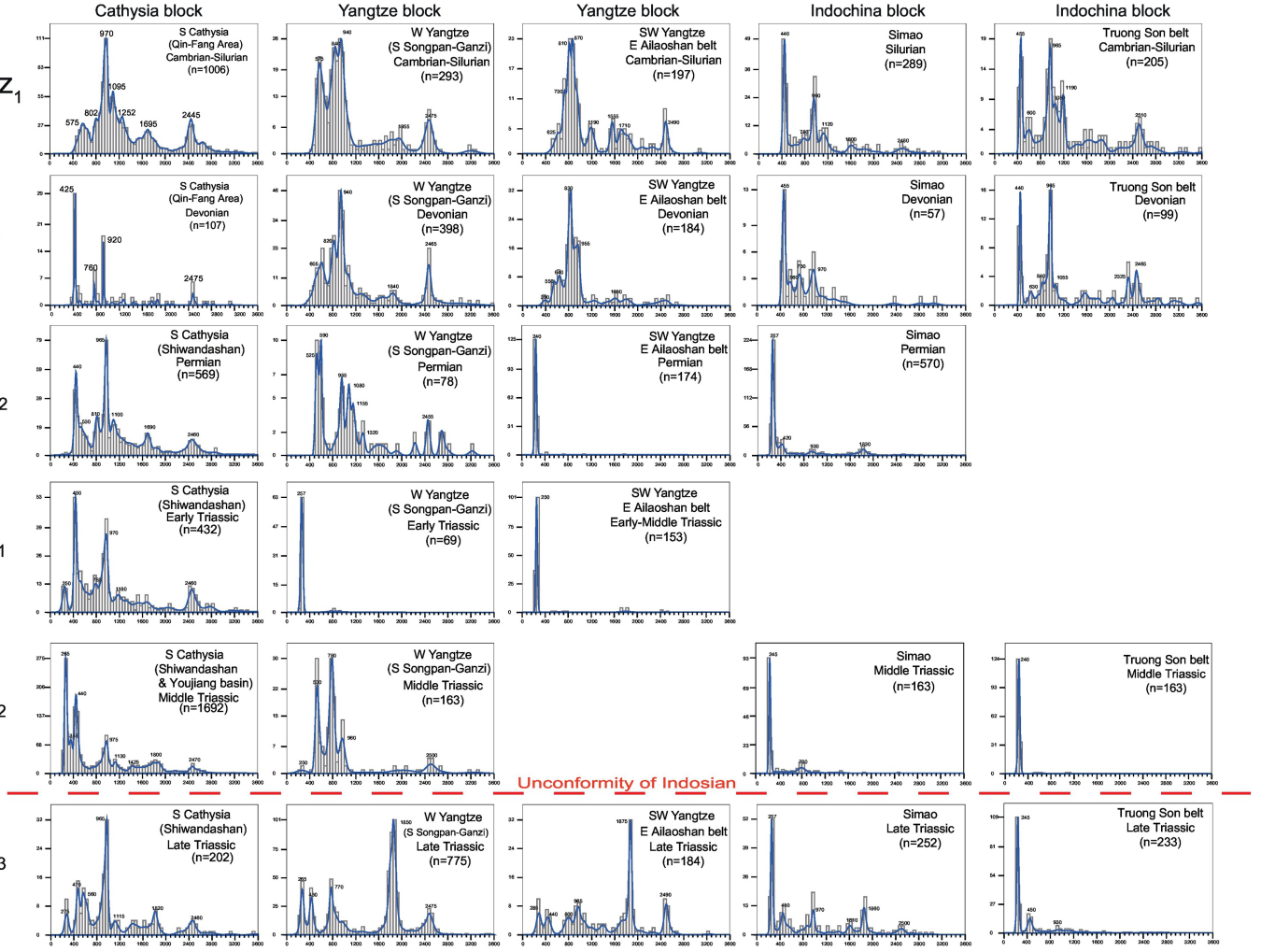
Cathysia block
Yangtze block
Yangtze block
Indochina block
Indochina block
Pz1
D
P2
T1
T2
T3
S Cathysia (Qin-Fang Area) Cambrian-Silurian (n=1006)
W Yangtze (S Songpan-Ganzi) Cambrian-Silurian (n=293)
SW Yangtze E Ailaoshan belt Cambrian-Silurian (n=197)
Simao Silurian (n=289)
Truong Son belt Cambrian-Silurian (n=205)
S Cathysia (Qin-Fang Area) Devonian (n=107)
W Yangtze (S Songpan-Ganzi) Devonian (n=398)
SW Yangtze E Ailaoshan belt Devonian (n=184)
Simao Devonian (n=57)
Truong Son belt Devonian (n=99)
S Cathysia (Shiwandashan) Permian (n=569)
W Yangtze (S Songpan-Ganzi) Permian (n=78)
SW Yangtze E Ailaoshan belt Permian (n=174)
Simao Permian (n=570)
S Cathysia (Shiwandashan) Early Triassic (n=432)
W Yangtze (S Songpan-Ganzi) Early Triassic (n=69)
SW Yangtze E Ailaoshan belt Early-Middle Triassic (n=153)
S Cathysia (Shiwandashan & Youjiang basin) Middle Triassic (n=1692)
W Yangtze (S Songpan-Ganzi) Middle Triassic (n=163)
Simao Middle Triassic (n=163)
Truong Son belt Middle Triassic (n=163)
Unconformity of Indosian
S Cathysia (Shiwandashan) Late Triassic (n=202)
W Yangtze (S Songpan-Ganzi) Late Triassic (n=775)
SW Yangtze E Ailaoshan belt Late Triassic (n=184)
Simao Late Triassic (n=252)
Truong Son belt Late Triassic (n=233)

Figure 15

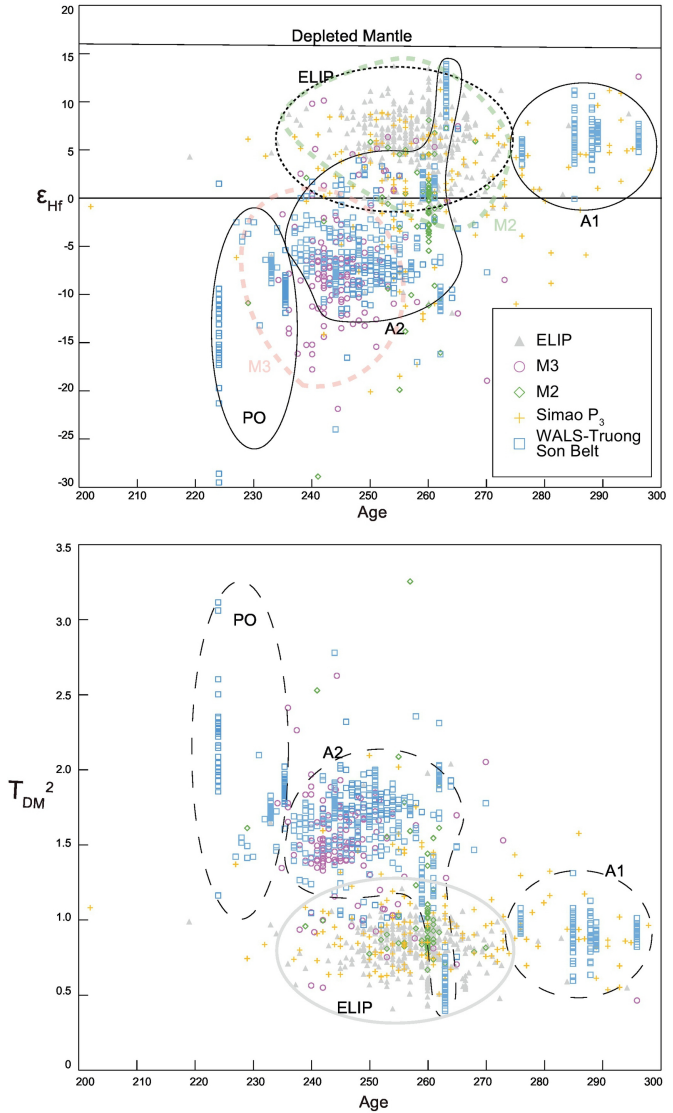
Depleted Mantle
ELIP
M2
A1
A2
M3
PO
ELIP
M3
M2
Simao P3
WALS-Truong Son Belt
εHf
Age
PO
A2
A1
ELIP
TDM2
Age

Figure 16

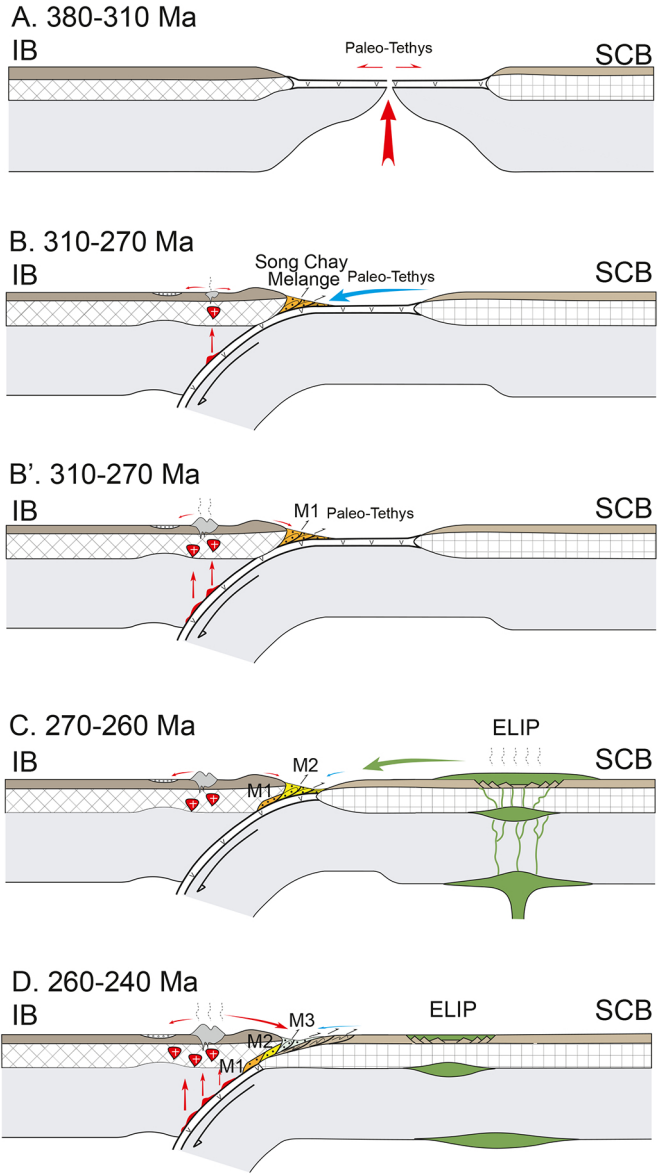
A. 380-310 Ma
IB
Paleo-Tethys
SCB
B. 310-270 Ma
IB
Song Chay
Melange
Paleo-Tethys
SCB
B'. 310-270 Ma
IB
M1
Paleo-Tethys
SCB
C. 270-260 Ma
IB
M2
M1
ELIP
SCB
D. 260-240 Ma
IB
M3
M2
M1
ELIP
SCB

Figure 17

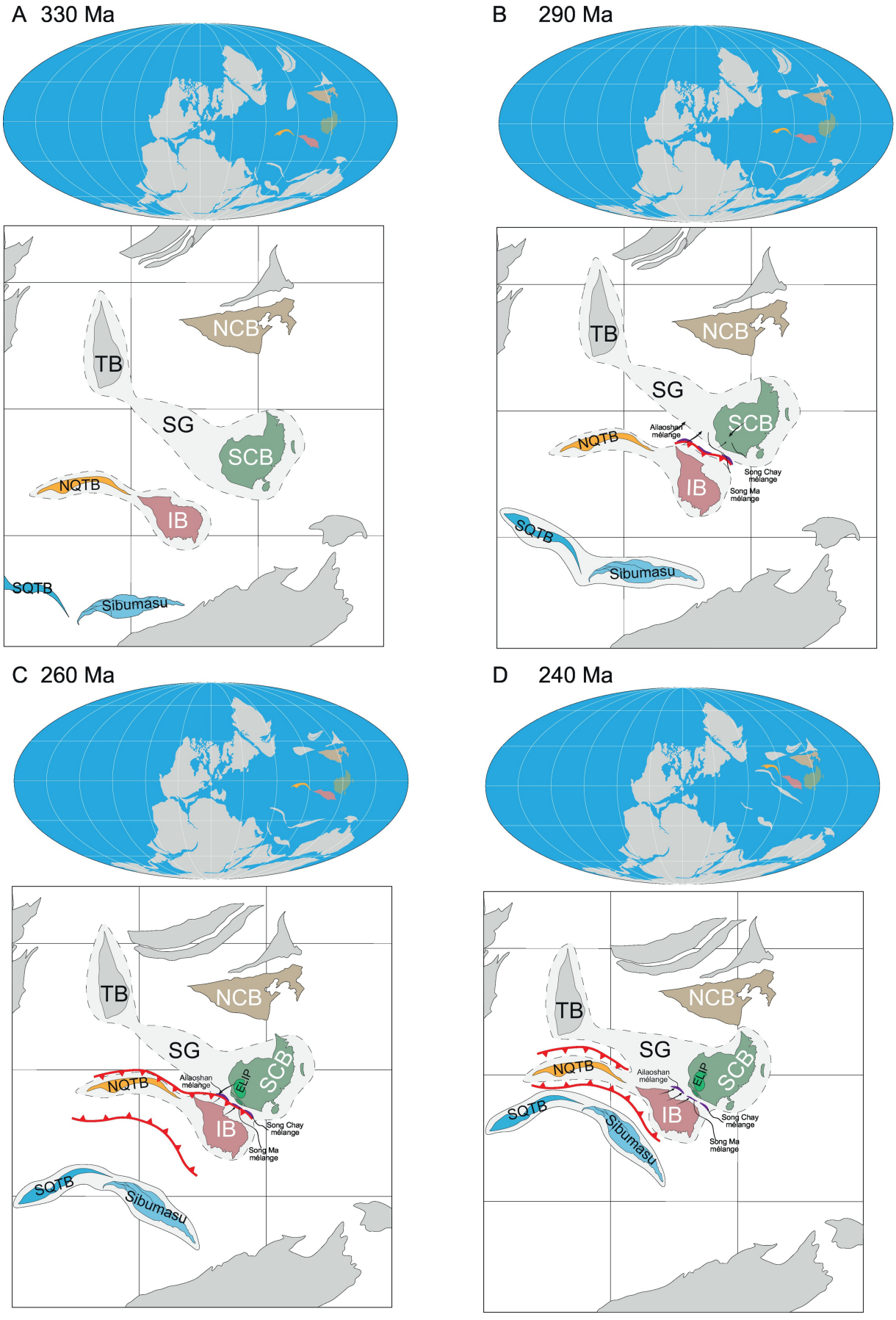
A 330 Ma
NCB
TB
SG
SCB
NQTB
IB
SQTB
Sibumasu
B 290 Ma
TB
NCB
SG
SCB
Ailaoshan mélange
NQTB
Song Chay mélange
IB
Song Ma mélange
SQTB
Sibumasu
C 260 Ma
TB
NCB
SG
NQTB
Ailaoshan mélange
ELIP
SCB
IB
Song Chay mélange
Song Ma mélange
SQTB
Sibumasu
D 240 Ma
TB
NCB
SG
NQTB
Ailaoshan mélange
ELIP
SCB
SQTB
IB
Song Chay mélange
Sibumasu
Song Ma mélange

Figure 18